Journal of Geodynamics 100 (2016) 7–32

Contents lists available at ScienceDirect

Journal of Geodynamics

journal homepage: http://www.elsevier.com/locate/jog

A review of analogue modelling of geodynamic processes: Approaches, scaling, materials and quantification, with an application to subduction experiments

Wouter P. Schellart[a,b,*], Vincent Strak[a,c]

[a] School of Earth, Atmosphere and Environment, Monash University, Melbourne VIC 3800, Australia
[b] Faculty of Earth and Life Sciences, Vrije Universiteit Amsterdam, Amsterdam, Netherlands
[c] Earthquake Research Institute, University of Tokyo, Tokyo, Japan

ARTICLE INFO

Article history:
Received 11 December 2015
Received in revised form 18 March 2016
Accepted 19 March 2016
Available online 21 May 2016

Keywords:
Analogue modelling
Geodynamics
Geology
Scaling
Topography
Topographic correction factor
Subduction
Rheology
Recording
Quantification

ABSTRACT

We present a review of the analogue modelling method, which has been used for 200 years, and continues to be used, to investigate geological phenomena and geodynamic processes. We particularly focus on the following four components: (1) the different fundamental modelling approaches that exist in analogue modelling; (2) the scaling theory and scaling of topography; (3) the different materials and rheologies that are used to simulate the complex behaviour of rocks; and (4) a range of recording techniques that are used for qualitative and quantitative analyses and interpretations of analogue models. Furthermore, we apply these four components to laboratory-based subduction models and describe some of the issues at hand with modelling such systems. Over the last 200 years, a wide variety of analogue materials have been used with different rheologies, including viscous materials (e.g. syrups, silicones, water), brittle materials (e.g. granular materials such as sand, microspheres and sugar), plastic materials (e.g. plasticine), visco-plastic materials (e.g. paraffin, waxes, petrolatum) and visco-elasto-plastic materials (e.g. hydrocarbon compounds and gelatins). These materials have been used in many different set-ups to study processes from the microscale, such as porphyroclast rotation, to the mantle scale, such as subduction and mantle convection. Despite the wide variety of modelling materials and great diversity in model set-ups and processes investigated, all laboratory experiments can be classified into one of three different categories based on three fundamental modelling approaches that have been used in analogue modelling: (1) The external approach, (2) the combined (external + internal) approach, and (3) the internal approach. In the external approach and combined approach, energy is added to the experimental system through the external application of a velocity, temperature gradient or a material influx (or a combination thereof), and so the system is open. In the external approach, all deformation in the system is driven by the externally imposed condition, while in the combined approach, part of the deformation is driven by buoyancy forces internal to the system. In the internal approach, all deformation is driven by buoyancy forces internal to the system and so the system is closed and no energy is added during an experimental run. In the combined approach, the externally imposed force or added energy is generally not quantified nor compared to the internal buoyancy force or potential energy of the system, and so it is not known if these experiments are properly scaled with respect to nature. The scaling theory requires that analogue models are geometrically, kinematically and dynamically similar to the natural prototype. Direct scaling of topography in laboratory models indicates that it is often significantly exaggerated. This can be ascribed to (1) The lack of isostatic compensation, which causes topography to be too high. (2) The lack of erosion, which causes topography to be too high. (3) The incorrect scaling of topography when density contrasts are scaled (rather than densities); In isostatically supported models, scaling of density contrasts requires an adjustment of the scaled topography by applying a topographic correction factor. (4) The incorrect scaling of

* Corresponding author.
E-mail address: wouter.schellart@monash.edu (W.P. Schellart).

http://dx.doi.org/10.1016/j.jog.2016.03.009

externally imposed boundary conditions in isostatically supported experiments using the combined approach; When externally imposed forces are too high, this creates topography that is too high. Other processes that also affect surface topography in laboratory models but not in nature (or only in a negligible way) include surface tension (for models using fluids) and shear zone dilatation (for models using granular material), but these will generally only affect the model surface topography on relatively short horizontal length scales of the order of several mm across material boundaries and shear zones, respectively.

1. Introduction

Analogue modelling (also referred to as laboratory modelling or physical modelling) is an experimental approach that is used in the Earth Sciences to investigate geological phenomena and geodynamic processes in a laboratory at convenient time scales and length scales. Analogue models are simplified representations of a particular component of the Earth's system (the natural prototype) using simplified geometries, rheologies and boundary conditions. Analogue models are useful because they overcome some inherent limitations that exist when studying the Earth directly. In particular, the study of geodynamic processes in nature is difficult because: (1) only the present state of the Earth is known; (2) Many geodynamic processes occur at geological time scales of millions of years, which far exceed the human life span; (3) Many geodynamic processes occur at large spatial scales and deep inside the Earth, making direct observation difficult or impossible. Analogue models allow one to investigate the progressive development of a particular geodynamic process or geological phenomenon from start to finish, providing a complete evolutionary picture of the process under investigation. Furthermore, such processes can be investigated in a controlled environment of the laboratory at convenient time scales (seconds to hours) and length scales (millimetres to meters). Additionally, analogue models allow the experimenter to systematically investigate and quantify the influence of a particular physical parameter on a particular geodynamic process. Finally, in case the model is properly scaled, then the experimental results can be directly applied to the natural prototype, providing insight into the natural system.

Analogue modelling has a long history, starting 200 years ago with the first analogue experiments conducted by Sir James Hall (Hall, 1815), who developed models to investigate the folding of layered sedimentary rocks. Other modellers followed in the late 1800s studying geological structures such as fractures, folds and thrust faults (e.g. Favre, 1878a,b; Daubre, 1879; Schardt, 1884; Cadell, 1889; Willis, 1893). An increase in analogue modelling studies occurred in the 1900s, as a larger diversity of geodynamic processes and geological phenomena were investigated, including salt dome formation (e.g. Escher and Kuenen, 1929; Link, 1930; Parker and McDowell, 1955), folding (e.g. Mead, 1920; Kuenen and de Sitter, 1938), thrust faulting (Hubbert, 1951), normal faulting (e.g. Hubbert, 1951), fracturing (e.g. Mead, 1920; Cloos, 1955; Oertel, 1962), proto-subduction (Kuenen, 1936), mantle flow (e.g. Griggs, 1939), orogeny (e.g. Kuenen, 1936; Griggs, 1939), boudinage (e.g. Ramberg, 1955), plutonism (e.g. Ramberg, 1970) and plume formation (e.g. Whitehead and Luther, 1975). As the theory of plate tectonics was developed in the 1960s, analogue models of plate tectonic processes followed, including the first analogue models of subduction (e.g. Jacoby, 1973, 1976; Kincaid and Olson, 1987), lithospheric rifting (e.g. Shemenda and Grocholsky, 1994; Benes and Davy, 1996; Brune and Ellis, 1997), collision-indenter tectonics (e.g. Tapponnier et al., 1982; Davy and Cobbold, 1988; Ratschbacher et al., 1991), and lithospheric shortening (e.g. Davy and Cobbold, 1991).

During the 1900s, analogue modelling changed from being a qualitative and descriptive tool to a quantitative technique due to the formulation of the scaling theory, which was first introduced by Hubbert (1937) and further developed by many others (e.g. Hubbert, 1951; Ramberg, 1967, 1981; Horsfield, 1977; Shemenda, 1983; Weijermars and Schmeling, 1986; Richard, 1991; Davy and Cobbold, 1991; Ribe and Davaille, 2013). The scaling theory, which requires geometric, kinematic and dynamic similarity between analogue model and natural prototype, allows the experimenter to scale quantitative model results such as lengths, geometries, velocities, forces, stresses and strains to values in nature, allowing for a quantitative and deeper understanding of the geological phenomenon or geodynamic process under investigation.

The analogue modelling technique has come a long way in the last 200 years, and has provided many novel insights into a wide variety of geological phenomena and geodynamic processes. In the last decade, the reproducibility of analogue models has been under investigation with benchmark studies of upper crustal shortening and extension (Schreurs et al., 2006), and upper crustal shortening (Schreurs et al., 2016). Such studies provide new insight into the influence of a variety of conditions (e.g. lab environment, experimental apparatus, analogue materials, model preparation techniques, the human factor) on the experimental outcomes and reproducibility of analogue experiments.

In the last three decades a number of reviews have been written on analogue modelling of particular geodynamic settings and processes, including extensional fault systems (McClay, 1990), continental extension (Corti et al., 2003), accretionary wedges (Graveleau et al., 2012), strike-slip zones (Dooley and Schreurs, 2012) and mantle convection (Davaille and Limare, 2007). In addition, a number of reviews exist on the history of analogue modelling (e.g. Koyi, 1997; Ranalli, 2001; Schellart, 2002).

This review work on analogue modelling is more general than the above-mentioned reviews, although it does provide an application to analogue modelling of subduction. Note that this review will only focus on analogue modelling performed in the normal field of gravity. So far, most analogue models have been performed in the normal (Earth's) field of gravity, although a considerable number of models have also been performed in an artificial gravity field, such as induced by a centrifuge (e.g. Ramberg, 1967; Dixon and Summers, 1985; Peltzer, 1988; Bonini et al., 2001; Harris and Koyi, 2002; Mart et al., 2005; Corti et al., 2010; Dietl and Koyi, 2011; Noble and Dixon, 2011; Godin et al., 2011).

The review has four main aims. The first is to provide a fundamental physical classification scheme for the three different analogue modelling approaches that exist, to discuss for which geodynamic problem each of these approaches might be justified or not, and to discuss potential problems and limitations with these different approaches. The second aim is to provide a discussion and new insight into the scaling of topography in analogue models. It will be shown, using the scaling theory, that topography in analogue experiments needs to be scaled differently in case the experiments are scaled for density contrasts instead of densities. The third aim is to provide an overview of the different rheological approaches that have been used in analogue modelling to represent

the rheological layering of the Earth, and to discuss the advantages and inherent limitations of each of these rheological approaches. The fourth and final aim is to provide an overview of the different recording and visualisation techniques that have been used in analogue modelling to provide qualitative and quantitative insight into geodynamic processes on Earth.

2. Analogue modelling approaches

In analogue modelling of geodynamic processes, three fundamental approaches exist, depending on how deformation in the system is driven: externally (open system), internally (closed system), and both externally and internally (open system) (Fig. 1). Below we will describe these three different approaches, explain the reasons for using them, and discuss how they are suited (or not) to different research questions.

2.1. External approach

In the first approach, deformation in the model is driven entirely by externally applied boundary conditions. This means that during the course of an experiment, energy is added to the experimental system, and so the system is open. Thus, the experimenter imposes the experimental conditions both initially and continuously. It is this externally added energy that is the driver of deformation or flow in the experiment. We will refer to this approach as the external approach and to models that use this approach as externally-driven models. The most commonly used external boundary conditions are velocity boundary conditions (kinematic external approach), thermal boundary conditions (thermal external approach), and material influx conditions (material influx external approach).

In the kinematic external approach, internal buoyancy forces play no (or at most a negligible) role in driving deformation or flow in the model. Examples of this type of approach include sandbox experiments that focus on upper crustal deformation, in which shearing and faulting of frictional-plastic granular material such as sand and glass microspheres are driven entirely by the externally imposed velocity boundary conditions. Such experiments investigated strike-slip deformation (e.g. Naylor et al., 1986; McClay and Dooley, 1995; Schellart and Nieuwland, 2003; Dufréchou et al., 2011; Dooley and Schreurs, 2012), extension (e.g. McClay, 1990; Keep and McClay, 1997), thrust and accretionary wedge formation (e.g. Lallemand et al., 1992; Koyi, 1995; Gutscher et al., 1998; Dominguez et al., 1998; Storti et al., 2000; Kukowski et al., 2002; Hampel et al., 2004; Schreurs et al., 2006; Bose et al., 2015), transpression (e.g. Leever et al., 2011), and thrust-strike-slip interference (e.g. Duarte et al., 2011; Rosas et al., 2012, 2015). Examples of lithospheric scale experiments using a kinematic external approach include indenter-extrusion experiments (e.g. Tapponnier et al., 1982), while examples of mantle-scale experiments include a number of subduction experiments in which slab motion is externally controlled (e.g. Buttles and Olson, 1998; Kincaid and Griffiths, 2003, 2004; Druken et al., 2011; MacDougall et al., 2014). There are also many experiments that focus on microscale or mesoscale (outcrop scale) processes that use the kinematic external approach, such as experiments that focus on shear zone formation (e.g. Ildefonse et al., 1992; Grujic and Mancktelow, 1998; Mancktelow et al., 2002), porphyroclast rotation (e.g. Passchier and Sokoutis, 1993), folding (e.g. Abbassi and Mancktelow, 1992; Rosas et al., 2002; Marques et al., 2008; Dell'Ertole and Schellart, 2013; Ramón et al., 2013), and boudinage (e.g. Zulauf et al., 2011; Marques et al., 2012).

In the thermal external approach, a temperature gradient (usually vertical) is externally imposed on (part of) one or more of the experimental box boundaries, which imposes a density gradient in the experimental material. Such a density gradient can then lead to convection with the formation of convective rolls and/or plume formation (e.g. Busse and Whitehead, 1971; White, 1988; Weinstein and Olson, 1990; Weinstein and Christensen, 1991; Davaille and Jaupart, 1993; Weeraratne and Manga, 1998) or subduction (e.g. Jacoby, 1976). In such experiments, buoyancy forces drive all the deformation and flow, but the buoyancy forces are generated by externally imposed conditions during the experiment.

In the material influx external approach, material is progressively added to the experimental domain, which drives the deformation or flow. Examples of this approach are magma intrusion and dike formation experiments (e.g. Donnadieu and Merle, 1998; Mathieu et al., 2008; Kervyn et al., 2009; Galland et al., 2009; Norini and Acocella, 2011; Rivalta et al., 2015), volcano inflation and/or deflation experiments (e.g. Acocella et al., 2000; Tibaldi et al., 2008), and mantle plume experiments in which a compositionally buoyant fluid is progressively injected into the base of a tank containing a higher-density fluid (e.g. Whitehead and Luther, 1975). In these experiments, buoyancy forces originating from the density contrast between the injected fluid and the ambient material, as well as the pressure gradient at the injection point, drive deformation and flow in the experimental box.

Different combinations of two of the above-mentioned three approaches exist as well. These include experiments that combine the thermal and material influx external approaches, in which a cold (negatively buoyant) slab-like fluid or a hot (positively buoyant) plume-like fluid is injected in the experimental tank (e.g. Griffiths et al., 1995; Guillou-Frottier et al., 1995; Griffiths, 1986; Griffiths and Campbell, 1990). Other experiments exist that combine the kinematic and thermal external approaches, with externally imposed motion at the top and/or bottom of a tank causing mantle shearing and heating/cooling at the base/top of the tank inducing mantle convection and/or plume formation (e.g. Richter and Parsons, 1975; Jellinek et al., 2003; Kerr and Mériaux, 2004). Experiments that combine the kinematic and material influx external approaches include kinematically-driven thrust wedge experiments in which a fluid is injected at the base to simulate magma intrusion during thrusting (e.g. Galland et al., 2003; Montanari et al., 2010), and models of subduction-induced mantle plume deflection in which a rigid kinematically-controlled slab deflects a mantle plume injected at the base of the tank (e.g. Druken et al., 2014).

2.2. Combined (external + internal) approach

In the second approach, deformation in the model is driven partly by externally imposed boundary conditions and partly by internal buoyancy forces. As with the first approach, this means that during the course of an experiment, energy is added to the experimental system, and so the system is open, and the experimenter imposes the experimental conditions both initially and continuously. However for the second approach, deformation and flow in the experiment is driven both by the externally added energy and by the energy internal to the system (potential energy). We will refer to this approach as the combined (or external + internal) approach and to models that use this approach as externally + internally-driven models. The most commonly used external boundary conditions for the combined approach are velocity boundary conditions (kinematic combined approach) and material influx conditions (material influx combined approach). Examples of upper crustal-scale experiments that use the combined approach include delta collapse experiments (e.g. McClay et al., 1998; Mourgues et al., 2009; Brun and Fort, 2011) and salt diapirism experiments (e.g. Warsitzka et al., 2013) that have internal buoyancy forces and include differential loading due to local syn-experimental sedimentation. Other upper crustal experi-

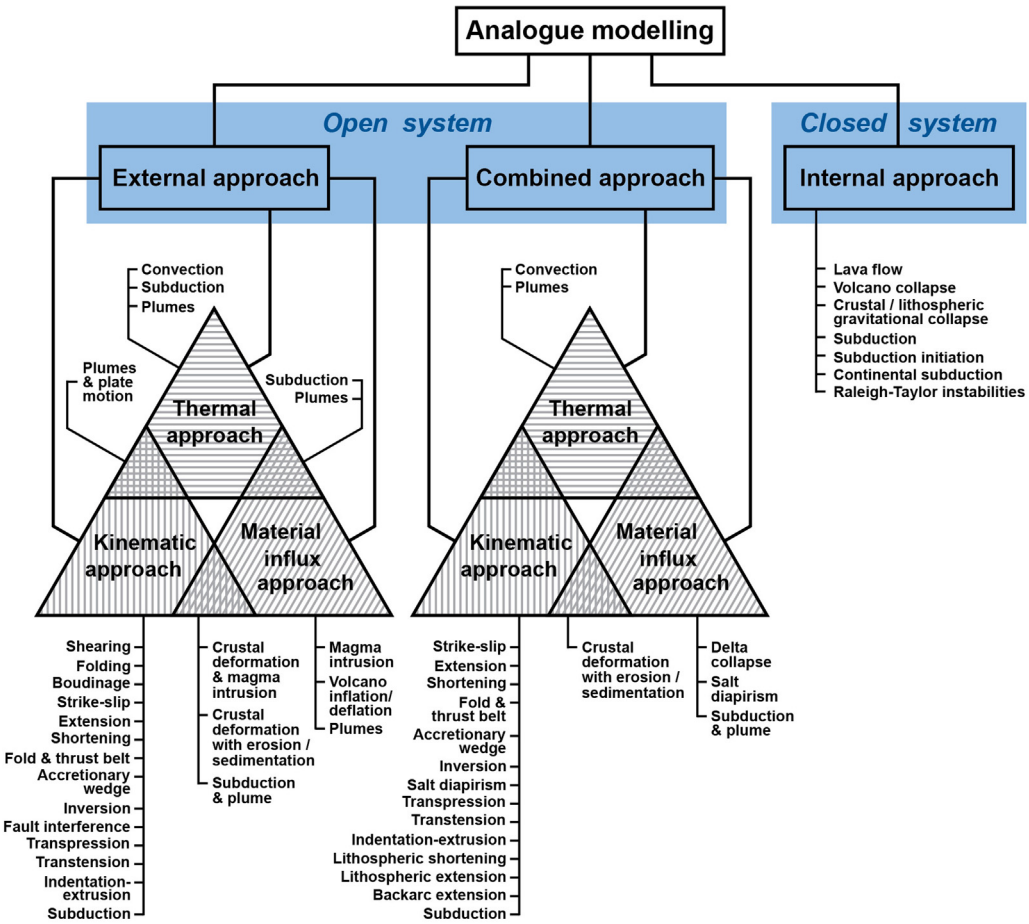

Fig. 1. Classification scheme illustrating the three fundamental approaches in analogue modelling of geological and geodynamic processes: The external approach (in which all deformation in the experimental system is driven by externally imposed boundary conditions), the combined approach (in which deformation in the experimental system is driven by both externally imposed boundary conditions and internal buoyancy forces) and the internal approach (in which all deformation in the experimental system is driven by internal buoyancy forces). The external and combined approaches each have three sub-approaches: the thermal approach, the kinematic approach and the material influx approach. Combinations of these sub-approaches exist as well. Numerous examples are given for each of the main approaches, the sub-approaches, and combinations thereof. See section 2 for a thorough discussion.

ments include kinematically-driven thrust experiments, extension experiment and transpression experiments with internal buoyancy forces due to inclusion of buoyant viscous layers below more dense brittle layers (e.g. Keep and McClay, 1997; Benn et al., 1998; Casas et al., 2001; Bahroudi and Koyi, 2003; Luján et al., 2006; Storti et al., 2007; Bonini, 2007; Nilforoushan and Koyi, 2007), as well as kinematically-driven extension experiments investigating salt diapirs (e.g. Vendeville and Jackson, 1992). Lithospheric-scale examples of this type of approach include a large number of experiments that combine externally-imposed kinematic boundary conditions and internal buoyancy forces, such as indentation-extrusion experiments (e.g. Davy and Cobbold, 1988; Ratschbacher et al., 1991; Martinod et al., 2000; Fournier et al., 2004; Regard et al., 2005), lithospheric shortening experiments (e.g. Davy and Cobbold, 1991; Buck and Sokoutis, 1994; Keep, 2000, 2003; Moore et al., 2005a,b; Marques, 2008; Willingshofer and Sokoutis, 2009; Luth et al., 2013a; Calignano et al., 2015), lithospheric extension experiments (e.g. Benes and Davy, 1996; Brune and Ellis, 1997; Corti, 2008; Autin et al., 2010), and backarc extension experiments (e.g. Schellart et al., 2002a,b; Schellart et al., 2003). Examples of mantle-scale experiments include a variety of subduction experiments with negatively buoyant slabs in which the rate of plate motion is externally controlled by one or more pistons (e.g. Shemenda, 1992, 1993; Faccenna et al., 1999; Regard et al., 2003; Boutelier et al., 2003; Schellart, 2005; Heuret et al., 2007; Guillaume et al., 2009; Göğüş et al., 2011; Martinod et al., 2013; Bajolet et al., 2013; Agard et al., 2014), experiments that include buoyancy-driven subduction and externally-controlled plume injection (e.g. Mériaux et al., 2015a, 2015b), and thermo-chemical convection and plume formation experiments, where motions in the system are driven by temperature gradients applied externally and by internal density heterogeneities of chemical origin (Davaille et al., 2002; Le Bars and Davaille, 2004; Kumagai et al., 2007).

2.3. Internal approach

In the third approach, internal buoyancy forces that are present in the experiment itself drive all the deformation and motion. We will refer to this approach as the internal approach, and models using this approach as internally-driven models. Thus, in internally-driven models the experimenter imposes the experimental conditions only initially. Internally-driven models are often referred to as either fully dynamic models, self-consistent models or buoyancy-driven models (but note that there are also buoyancy-driven models that use the thermal external approach or combined approach, see Section 2.1 and Section 2.2). In internally-driven models, no external (non-zero) velocities, forces or temperature gradients are applied and no materials are added to the experimental system. As such, no energy is added to the system during

the experiment, meaning that energy is conserved and the system is closed. Examples of internally-driven models include crustal and lithospheric gravitational collapse/spreading models (e.g. Merle, 1989; Hatzfeld et al., 1997; Gautier et al., 1999; Schellart and Lister, 2005), gravitational lava flow models (e.g. Lyman et al., 2005; Applegarth et al., 2010), volcano collapse models (e.g. Platz et al., 2011), buoyancy-driven subduction initiation experiments (e.g. Goren et al., 2008), buoyancy-driven subduction models (e.g. Jacoby, 1973; Kincaid and Olson, 1987; Funiciello et al., 2003, 2006, 2008; Schellart, 2004a, 2008, 2010a,b; Bellahsen et al., 2005; Guillaume et al., 2009, 2010; Duarte et al., 2013; Strak and Schellart, 2014; Chen et al., 2015a,b, 2016), buoyancy-driven continental subduction experiments (e.g. Edwards et al., 2015), and experiments investigating Rayleigh-Taylor instabilities (e.g. Whitehead and Luther, 1975; Bercovici and Kelly, 1997).

2.4. Thoughts and remarks on different approaches

The choice of model approach depends on the scientific question that the experimenter wants to address. In case the experimenter wants to investigate the evolution of deformation in a relatively small-scale system, which itself lacks the energy to drive this deformation (e.g. an upper crustal strike-slip system or a millimetre-scale shear zone), then an external approach is entirely justified. Indeed, in such a system, far-field forces (e.g. plate tectonic) are responsible for such deformation and so an externally imposed driver is essential. If, however, an experimenter wants to investigate a larger-scale (e.g. upper mantle or whole mantle) process such as slab deformation during subduction, then internal slab buoyancy forces play a major role in the slab's own deformation, and so an external approach is not justified. The question then remains, would an internal approach be justified, a combined approach, or both. This again depends on the scientific question that the experimenter wants to address. For example, if the experimenter wishes to investigate whether local subduction can drive local overriding plate deformation, then an internal approach is required. However, if the experimenter wishes to investigate one subduction system attached to a very large tectonic plate that is itself attached to several other subduction systems (e.g. Pacific plate with Aleutians-Alaska, Kamchatka-Kuril-Japan-Izu-Bonin-Mariana and Tonga-Kermadec-Hikurangi subduction zones), then a combined approach would be justified as long as the externally imposed force is quantified and scaled with respect to the internal buoyancy forces of the system. Unfortunately, experimental studies that use the combined approach generally do not quantify the externally-imposed force or energy component to see if it properly scales with the buoyancy force or potential energy internal to the system. Such quantification, however, is essential for modelling of large-scale systems such as subduction systems, where externally + internally-driven subduction can lead to very different results compared to internally-driven subduction, as will be discussed below.

2.5. Model approaches in subduction experiments

The first laboratory-based subduction models have been developed in the 1970s (Jacoby, 1973, 1976), and were preceded by pre-plate tectonics models that contained certain elements of subduction (Kuenen, 1936). The models from Jacoby (1973) were entirely buoyancy driven using the internal approach and started with a small slab perturbation that progressively grew. The models excluded an overriding plate and used relatively simple rheologies for the slab (rubber) and sub-lithospheric mantle (water). The models that followed were buoyancy-driven thermo-mechanical models with an externally imposed temperature gradient, which also lacked an overriding plate (Jacoby, 1976). Kincaid and Olson (1987) presented subduction experiments excluding an overriding plate, but also presented the first subduction experiments with an overriding plate using a buoyancy-driven internal approach. The models used viscous sucrose solution materials to model the plates and the sub-lithospheric mantle, and started with a short initial slab perturbation to drive subduction. The experiments with an overriding plate, however, started with a large, 0.5–2.5 cm, gap between overriding plate and subducting plate, scaling to ~50–250 km in their experiments (using a length scaling where 1 cm in the experiment represents 100 km in nature).

The first laboratory models of subduction in which the subducting and overriding plates were in physical contact were developed by Shemenda (1992, 1993) using a combined approach, in which plate motion was driven by one or more pistons. Other modellers followed suite, also using a combined approach (e.g. Faccenna et al., 1999; Regard et al., 2003; Boutelier et al., 2003). Shemenda (1992) investigated subduction initiation and progressive subduction evolution using undeformed lithosphere, either laterally homogeneous or heterogeneous, or pre-cut lithosphere. Faccenna et al. (1999) and Regard et al. (2003) investigated subduction initiation and progressive subduction evolution using undeformed, laterally heterogeneous, lithosphere. More recently subduction models were developed that used a geometric set-up comparable to that of Kincaid and Olson (1987), thus including an overriding plate and starting with a short subduction perturbation, but that used a combined approach with one or two external pistons to drive plate motion (e.g. Heuret et al., 2007; Guillaume et al., 2009; Martinod et al., 2013; Agard et al., 2014).

Although the combined approach as discussed in the previous paragraph could be justified in certain cases of subduction experiments, a major problem is that in such experiments it is generally never quantified how much energy or force the externally imposed velocity adds to the experimental system. Consequently, it is not known if the imposed force and energy are properly scaled with respect to the internal buoyancy forces and potential energy in the system. Unfortunately, this problem is generally never acknowledged nor discussed. For example, if one assumes that the externally imposed push force from a piston represents a ridge push force, then, considering that the ridge push force is about an order of magnitude smaller than the slab negative buoyancy force (e.g. Forsyth and Uyeda, 1975; Schellart, 2004b), the piston push force should be about an order of magnitude smaller than the slab negative buoyancy force in the experimental system.

We can discuss the issue at hand with two examples of subduction modelling and overriding plate deformation that use a different approach, namely the combined approach (Heuret et al., 2007) and the internal approach (Meyer and Schellart, 2013). Both use upper mantle subduction models with linear-viscous materials for the plates and the sub-lithospheric mantle. The scaled (trench-parallel) slab width in Meyer and Schellart (2013) is less (750 km) than in Heuret et al. (2007) (1800 km), but both can be considered narrow (Schellart et al., 2007). We do note that the subducting plate to sub-lithospheric upper mantle viscosity ratio (η_{SP}/η_{UM}) is lower in Meyer and Schellart (2013) (2.0×10^2) than in Heuret et al. (2007) (1.2×10^4). Also, Meyer and Schellart (2013) use a different lubrication layer at the subduction zone interface (honey diluted with water that has a nearly Newtonian viscosity of ~6 Pa s) compared to Heuret et al. (2007), who use Vaseline, which likely has a visco-plastic rheology (although its rheology is not described in their paper).

In Heuret et al. (2007), convergence between the subducting plate and overriding plate is externally controlled with pistons, and subduction occurs both through the externally imposed velocity boundary conditions applied to the plates and internal buoyancy forces of the negatively buoyant slab. It has not been quantified how the externally imposed forces compare and scale with the internal buoyancy forces. Heuret et al. (2007) find that with trench-

ward overriding plate motion and trench retreat the overriding plate shortens, and that with increasing trenchward overriding plate velocity, and increasing trench retreat velocity, the trench-normal overriding plate shortening rate increases. In other words, in their experiments, fast trench retreat corresponds to fast overriding plate shortening, while fast trench advance corresponds to overriding plate extension (their Fig. 5). These results are very much in contrast with the results of Meyer and Schellart (2013), who use models in which subduction, plate motion, mantle flow and overriding plate deformation are driven entirely by the slab negative buoyancy force (internal approach). These buoyancy-driven models show that trench retreat and trenchward overriding plate motion correspond with trench-normal overriding plate extension, and that with increasing trench retreat velocity, the extension rate in the overriding plate increases (their Fig. 7b).

The example above illustrates how, by using two different modelling approaches, one can reach two opposite (and conflicting) conclusions. The internal approach implies that overriding plate deformation is ultimately caused by the slab negative buoyancy force, which drives slab rollback, trench migration and mantle flow. The external approach implies that overriding plate motion drives its own deformation. The obvious question that remains then is, what drives overriding plate motion? Another important question that remains is, are the externally imposed forces that drive the overriding plate motion realistic in terms of magnitude when compared to the internal buoyancy forces? There is one important line of evidence that implies that, in general, the externally imposed forces in laboratory models of subduction, as well as those in models of lithospheric shortening and collision, are too high. This line of evidence is based on the topography observed in these models, which is too high. We will discuss this in more detail in Section 3.2.

3. Scaling

3.1. General scaling principles

Hubbert (1937) was the first to develop a well-founded scaling theory for analogue modelling of geological phenomena and geodynamic processes. This theory allowed for the first time to quantitatively compare laboratory experiments and their natural counterpart. Since Hubbert (1937), other papers have been published on scaling of analogue models (e.g. Hubbert, 1951; Ramberg, 1967, 1981; Horsfield, 1977; Shemenda, 1983; Weijermars and Schmeling, 1986; Davy and Cobbold, 1991; Ribe and Davaille, 2013). According to Hubbert (1937), there are three similarity criteria, which have to be fulfilled, in order for the model to be properly scaled. These criteria include geometric similarity, kinematic similarity and dynamic similarity. An analogue model and a natural prototype are geometrically similar if all the corresponding lengths (l_n, with n = 1, 2, 3,...) are proportional and all the corresponding angles (α_n) are equal in the model (superscript m) and natural prototype (superscript p):

$$\frac{l_1^m}{l_1^p} = \frac{l_2^m}{l_2^p} = \frac{l_3^m}{l_3^p} = \frac{l_n^m}{l_n^p} \tag{1a}$$

$$\frac{\alpha_1^m}{\alpha_1^p} = \frac{\alpha_2^m}{\alpha_2^p} = \frac{\alpha_3^m}{\alpha_3^p} = \frac{\alpha_n^m}{\alpha_n^p} = 1 \tag{1b}$$

For kinematic similarity, the geometrically similar model and natural prototype have to undergo similar changes of shape and/or position, where the time (t) required for any change in the model is proportional to the corresponding change in the prototype (Ramberg, 1967). This requires that:

$$\frac{t_1^m}{t_1^p} = \frac{t_2^m}{t_2^p} = \frac{t_3^m}{t_3^p} = \frac{t_n^m}{t_n^p} \tag{2}$$

Considering that velocity is essentially a length scale divided by time, then one can scale experimental velocities to the natural prototype using the following formulation:

$$v^p = v^m \frac{l^p t^m}{l^m t^p} \tag{3}$$

Dynamic similarity requires a similar distribution of driving forces (e.g. gravitational body forces or externally imposed (far-field) forces) and resistive forces (frictional, viscous). On Earth, gravitational body forces drive plate tectonics and mantle convection, and are thus also the main driver of far-field tectonic forces, which requires the analogue modeller to include mass in the scaling rules. For the scaling of forces and stresses, analogue modellers have used scaling rules to either scale densities (e.g. Davy and Cobbold, 1991; Shemenda, 1992, 1993; Boutelier et al., 2003; Boutelier and Cruden, 2013; Calignano et al., 2015) or density contrasts (e.g. Jacoby, 1973; Funiciello et al., 2003; Schellart, 2004a; Meyer and Schellart, 2013; Duarte et al., 2013; Martinod et al., 2013; Chen et al., 2015a,b). Ribe and Davaille (2013) have shown that both approaches are valid. However, there are important implications for the scaling of topography, which indicate that topography scales differently using either the density approach or the density contrast approach (see Section 3.2). Apart from scaling densities or density contrasts, dynamic similarity also requires the scaling of rheology to properly scale the resistive forces. The reader is referred to Section 4 and Weijermars and Schmeling (1986) for a discussion.

To scale forces and stresses using densities one can use Cauchy's equation of motion for a continuous medium (Davy and Cobbold, 1991). This equation describes the balance of linear momentum as follows:

$$\rho \frac{D^2 x_i}{Dt^2} = \frac{\partial \sigma_{ij}}{\partial x_j} + \rho g_i \, (i, j = 1, 2, 3) \tag{4}$$

where ρ is the density, x is the position vector, t is the time, σ is Cauchy's stress tensor and g is the acceleration due to gravity. The suffixes refer to Cartesian vector and tensor components in a fixed spatial frame. For slow motions, as in geological and tectonic processes, the only forces to be considered are body forces (due to gravity) and surface forces (stresses). Therefore, inertial forces are negligible and the second derivative of x to time t in Eq. (4) is negligible. Rearrangement of Eq. (4) results in:

$$\partial \sigma_{ij} = -\rho g_i \partial x_j \tag{5}$$

Integration of Eq. (5), with the boundary condition $\sigma_{ij} = 0$ at $x_j = 0$ (for scaling of processes at the scale of the upper crust, lithosphere or mantle, normal and shear stresses at the Earth's surface are negligible compared to stresses at depth) leads to:

$$\sigma_{ij} = -\rho g_i x_j \tag{6}$$

Writing Eq. (6) for both the analogue model (superscript m) and the natural prototype (superscript p), and dividing the former by the latter leads to:

$$\frac{\sigma_{ij}^m}{\sigma_{ij}^p} = \frac{\rho^m g_i^m x_j^m}{\rho^p g_i^p x_j^p} \tag{7}$$

When the experiment is executed in a normal field of gravity, then gravity is the same for both the natural prototype and the model. For the description of scaling rules for analogue experiments executed in an artificial field of gravity (e.g. centrifuge experiments), the reader is referred to Ramberg (1967) and Peltzer (1988). Furthermore, if we consider that x is simply a length scale, then Eq. (7) can be simplified to:

$$\frac{\sigma_{ij}^m}{\sigma_{ij}^p} = \frac{\rho^m l^m}{\rho^p l^p} \tag{8}$$

Eq. (8) thus illustrates that, in case one scales experiments for densities, then stresses scale with the product of density and length. To scale for forces (F), one can write stress as a force divided by the square of a length scale, and thus, using Eq. (8), we get:

$$\frac{F^m}{F^p} = \frac{\rho^m (l^m)^3}{\rho^p (l^p)^3} \tag{9}$$

Thus, in case one scales experiments for densities, forces scale with the product of density and the cube of length.

To scale forces and stresses using density contrasts one can use Stokes' settling law for sinking of a rigid object into an infinite volume fluid at very low Reynolds number (Jacoby, 1973; Duarte et al., 2013):

$$v \sim C \frac{\Delta \rho l^2 g}{\eta} \tag{10}$$

where $\Delta\rho$ is the density contrast between the sinking object and ambient fluid and C is a constant. Dynamic similarity requires that driving forces and resistive forces are proportional in the analogue model and natural prototype, which requires that:

$$\frac{\Delta \rho^m (l^m)^2 g^m}{\eta^m v^m} = \frac{\Delta \rho^p (l^p)^2 g^p}{\eta^p v^p} \tag{11}$$

We can rewrite Eq. (11) in terms of viscosity ratio. Furthermore, for experiments conducted in the normal field of gravity, then $g^m = g^p$. Finally, considering that velocity is simply a length scale over time, we get:

$$\frac{\eta^m}{\eta^p} = \frac{\Delta \rho^m l^m t^m}{\Delta \rho^p l^p t^p} \tag{12}$$

Because viscosity is a measure of stress divided by strain rate, and strain rate scales with the inverse of time, we can write Eq. (12) in terms of stress, leading to:

$$\frac{\sigma^m}{\sigma^p} = \frac{\Delta \rho^m l^m}{\Delta \rho^p l^p} \tag{13}$$

Eq. (13) thus illustrates that, in case one scales experiments for density contrasts, then stresses scale with the product of density contrast and length. To scale for forces (F), one can write stress as a force divided by the square of a length scale, and thus, using Eq. (13), we get:

$$\frac{F^m}{F^p} = \frac{\Delta \rho^m (l^m)^3}{\Delta \rho^p (l^p)^3} \tag{14}$$

Thus, in case one scales experiments for density contrasts, forces scale with the product of density contrast and the cube of length. In addition to scaling of stresses, forces, and viscosities, Eq. (11) can easily be reorganized to scale for velocities. If we assume again that experiments are conducted in the normal field of gravity ($g^m = g^p$), then we get:

$$\frac{v^m}{v^p} = \frac{\Delta \rho^m (l^m)^2 \eta^p}{\Delta \rho^p (l^p)^2 \eta^m} \tag{15}$$

3.2. Scaling of topography: why does topography often appear too high in analogue models?

The topography in analogue models generally appears too high and significantly exaggerated compared to the topography in the natural prototype. This is the case for upper crustal models such as thrust and accretionary wedge experiments, lithospheric models such as lithospheric shortening models, and mantle-scale models such as subduction models with an overriding plate. There are four main explanations for this topographic exaggeration: (1) The absence of isostatic compensation; (2) The scaling of density contrasts that requires the introduction of a correction factor for scaling of topography; (3) The incorrect scaling of applied external boundary conditions; (4) The absence of erosion. Below we will discuss these four explanations, as well as several other explanations that apply to relatively short length scales of topography.

3.2.1. Absence of isostatic compensation

Analogue models of upper crustal processes such as thrust and accretionary wedge experiments (e.g. Lallemand et al., 1992; Koyi, 1995; Dominguez et al., 1998; Storti et al., 2000; Hampel et al., 2004; Schreurs et al., 2006; Bose et al., 2015), transpression experiments (e.g. Leever et al., 2011), strike-slip experiments (e.g. Naylor et al., 1986; McClay and Dooley, 1995; Schellart and Nieuwland, 2003; Dufréchou et al., 2011; Dooley and Schreurs, 2012), extensional experiments (McClay, 1990), and thrust-strike-slip interference experiments (e.g. Duarte et al., 2011; Rosas et al., 2012, 2015) generally lack a low-viscosity fluid layer to provide isostatic compensation to the upper crustal layer. During the course of an upper crustal experiment, as deformation is externally driven, topography builds on top of a rigid base that does not subside (or move upwards) with an increased (or decreased) load of the deformed material due to thickening (or thinning). For example, in a typical double-vergent thrust wedge experiment from Storti et al. (2000) a topographic wedge develops with a maximum height of 5 cm (scaling to 5 km) and an extent of ~44 cm (scaling to 44 km) (measured perpendicular to the strike of the thrusts) after 52 cm of shortening (scaling to 52 km). Comparison to a natural analogue, the double-vergent Pyrenees mountain range, indicates a lower topography, with an average elevation of ~2.5 km in the highest part of the Eastern Pyrenees. The difference is particularly noticeable considering that estimates of shortening in the Eastern Pyrenees are some three times higher, 147–165 km (Muñoz, 1992; Fitzgerald et al., 1999), than the above mentioned analogue model, and the N-S extent of the orogen is ~150 km. The difference between model and natural prototype can be ascribed mostly to the lack of isostatic compensation in the upper crustal experiments, although a lack of erosion in most experiments also plays a role.

3.2.2. Scaling of densities or density contrasts and the topographic correction factor

In analogue experiments, the scaling of density contrasts or densities needs to be taken into account (see Section 3.1). In case an experiment contains different materials to represent different entities of the natural prototype with different densities, e.g. the continental crust (with ρ_{CC}), continental lithospheric mantle (with ρ_{CLM}), oceanic lithosphere (with ρ_{OL}) and sub-lithospheric upper mantle (with ρ_{SLUM}), then the ratios of density contrasts need to be proportional or, alternatively, the density ratios need to be proportional. For example, one could scale all the density contrasts in relation to ρ_{SLUM}:

$$\frac{\left(\rho^m_{SLUM} - \rho^m_{CC}\right)}{\left(\rho^P_{SLUM} - \rho^P_{CC}\right)} = \frac{\left(\rho^m_{SLUM} - \rho^m_{CLM}\right)}{\left(\rho^P_{SLUM} - \rho^P_{CLM}\right)} = \frac{\left(\rho^m_{SLUM} - \rho^m_{OL}\right)}{\left(\rho^P_{SLUM} - \rho^P_{OL}\right)} \tag{16}$$

Or in case one wants to scale densities, then:

$$\frac{\rho^m_{CC}}{\rho^p_{CC}} = \frac{\rho^m_{CLM}}{\rho^p_{CLM}} = \frac{\rho^m_{OL}}{\rho^p_{OL}} = \frac{\rho^m_{SLUM}}{\rho^p_{SLUM}} \tag{17}$$

In case one considers the formation of topography in laboratory models (and in nature), then this topography develops into the overlying fluid layer, the air layer. The overlying air layer is generally considered to provide a free surface boundary condition to the laboratory experiment (and to nature). In case one wants to relate the experimental topography to nature, then the density of air needs to be taken into account when scaling density contrasts or densities of the analogue materials. We can investigate

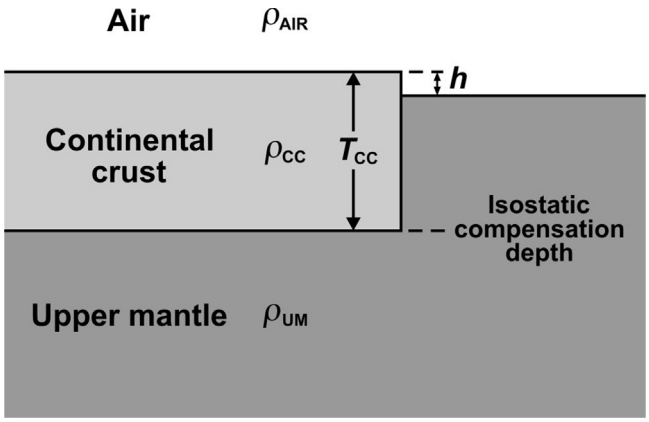

Fig. 2. Schematic diagram illustrating the principal of isostacy for a three-layer system. ρ_{AIR} is the density of the air, ρ_{CC} is the density of the continental crust and ρ_{UM} is the density of the upper mantle, with $\rho_{AIR} \ll \rho_{CC} < \rho_{UM}$. T_{CC} is the thickness of the continental crust and h is the difference in elevation between the top of the continental crustal layer and top of the mantle layer.

how topography in the experiment scales to nature in case either density contrasts or densities are scaled.

Consider a continental crustal layer with thickness T_{CC} and density ρ_{CC} that is resting on an upper mantle layer with uniform density ρ_{UM} (i.e. $\rho_{UM} = \rho_{CLM} = \rho_{SLUM}$) in isostatic equilibrium (Fig. 2). Because of isostacy, a column of material with a lighter crustal layer will have an elevation h with respect to a column with denser mantle material. At the depth equivalent to the base of the crustal layer the pressure will be equal for a column of crustal material and for a column of mantle material + air layer (i.e. the isostatic compensation depth):

$$\rho_{CC} g T_{CC} = \rho_{UM} g (T_{CC} - h) + \rho_{AIR} g h \tag{18}$$

Rearranging to solve for the elevation h, one gets:

$$h = T_{CC} \frac{(\rho_{UM} - \rho_{CC})}{(\rho_{UM} - \rho_{AIR})} \tag{19}$$

The density of air ρ_{AIR} is ~1.20 kg/m^3 (at 20 °C) and thus some three orders of magnitude smaller than ρ_{UM}, which is generally in the range 1000–1600 kg/m^3 in experiments and 3200–3400 kg/m^3 in nature. As such it appears justified to remove this parameter from the above equation, which can thus be simplified to:

$$h = T_{CC} \frac{(\rho_{UM} - \rho_{CC})}{\rho_{UM}} \tag{20}$$

To investigate how h in the experimental model relates to h in the natural prototype we can write:

$$\frac{h^m}{h^p} = \frac{T_{CC}^m}{T_{CC}^p} \frac{\rho_{UM}^p \left(\rho_{UM}^m - \rho_{CC}^m\right)}{\rho_{UM}^m \left(\rho_{UM}^p - \rho_{CC}^p\right)} \tag{21}$$

If we rearrange this equation in terms of the scaled elevation in nature h^p and if we consider that the ratio for crustal thickness is just a length scale ratio l^m/l^p, then we get:

$$h^p = C_{Topo} \frac{l^p}{l^m} h^m \tag{22}$$

with the topographic correction factor:

$$C_{Topo} = \frac{\rho_{UM}^m \left(\rho_{UM}^P - \rho_{CC}^p\right)}{\rho_{UM}^p \left(\rho_{UM}^m - \rho_{CC}^m\right)} \tag{23}$$

In case the density contrasts in the model and natural prototype are the same, then the topographic correction factor simplifies to:

$$C_{Topo} = \frac{\rho_{UM}^m}{\rho_{UM}^p} \tag{24}$$

The correction factor as shown in Eqs. (23) and (24) thus applies to experiments that scale density contrasts rather than densities. The density for model and nature that should be chosen to calculate C_{Topo} should be the one for the material that is located below the isostatic compensation depth that provides isostatic support, e.g. the upper mantle for the example discussed above or the asthenosphere or the sub-lithospheric upper mantle in case one considers a lithospheric layer (rather than just a crustal layer as in the example above).

For experiments that scale densities rather than density contrasts, a topographic correction is not required. This can be illustrated by rearranging Eq. (20) to:

$$h = T_{CC} \left(1 - \frac{\rho_{CC}}{\rho_{UM}}\right) \tag{25}$$

For experiments where the density ratios are scaled, ρ_{CC}/ρ_{UM} is the same for experiment and nature, and thus $(1-\rho_{CC}/\rho_{UM})^m = (1-\rho_{CC}/\rho_{UM})^p$. To investigate how h in the analogue model relates to h in the natural prototype we can now write:

$$\frac{h^m}{h^p} = \frac{T_{CC}^m}{T_{CC}^P} \tag{26}$$

If we consider again that the ratio for crustal thickness is just a length scale ratio l^m/l^p, and after rearranging, we get:

$$h^p = \frac{l^p}{l^m} h^m \tag{27}$$

If we compare this equation with Eq. (22) then we observe that the topographic correction factor C_{Topo} is missing. Thus, experiments in which the densities are scaled do not require a topographic correction and the observed topography can be directly scaled to topography in nature using Eq. (27). For experiments in which the density contrasts are scaled a topographic correction is required when scaling the experimental topography to nature and Eq. (22) should be used.

3.2.3. *Quantification and scaling of the applied external boundary conditions*

In isostatically compensated models with a free surface, topography develops during progressive deformation. The development of such topography appears particularly significant in those models that use the combined approach (e.g. Davy and Cobbold, 1991; Burg et al., 2002; Moore et al., 2005a,b; Cruden et al., 2006). In recent times, the recording of analogue models has made a major step forward through the 3D quantification of surface topography. For example, externally+internally-driven laboratory models of lithospheric deformation (e.g. Willingshofer and Sokoutis, 2009; Dombrádi et al., 2010; Luth et al., 2013a; Calignano et al., 2015) and subduction (e.g. Martinod et al., 2013) have been presented, illustrating the evolution of the three-dimensional surface topography with digital elevation models. Such digital elevation models provide a wealth of new, quantitative, data that can help understand the geodynamic processes under investigation. Nevertheless, this new quantitative tool in analogue modelling does highlight a new challenge for the analogue modelling community. In case the surface topography as illustrated in these digital elevation models is directly scaled to nature, then it becomes evident that the surface topography is often significantly exaggerated. Thus the questions arise as to what might be the origin of such exaggerated topography, and what might be the way forward in the analogue modelling community to produce models with scaled topographies that are more comparable to nature.

We will illustrate the above by discussing two recent examples of lithosphere-mantle scale experiments in which the surface topography has been accurately quantified. In the first exam-

ple, Calignano et al. (2015) present intraplate continental orogeny experiments that include internal buoyancy forces and externally imposed velocity boundary conditions (piston) that drive convergence. The authors have quantified the topography, which reaches 12–13 mm in several of their experiments, scaling to 24–26 km using their length scale ratio (1 cm represents 20 km, e.g. see their Figs. 3 and 4). The question arises as to what might drive the formation of such extreme topography in their experiments, in particular considering that they compare it to the Pyrenees with a topography that is an order of magnitude lower?

In the second example, Martinod et al. (2013) present subduction experiments that include an overriding plate and buoyancy forces, and for which trenchward overriding plate motion is externally driven using a velocity boundary condition (piston). The authors have quantified the topography of the overriding plate, up to 6 mm at the leading edge and −3 mm in the "backarc" region (their Fig. 13). These values scale to topographies in nature of 40 km for the leading edge of the overriding plate and −20 km for the backarc (in their models 1 cm represents 66 km). The elevated topography is about an order of magnitude higher than that observed in nature. Indeed, the South American subduction zone, to which the models are applied, has a mountain range at the leading edge of the overriding South American plate that has a maximum average elevation in the Central Andes of ~4 km (Altiplano). So the question arises again as to what might drive the formation of such extreme topography of up to 40 km in these laboratory models?

The above mentioned experiments are all isostatically compensated, and so the extreme topographies cannot be explained by the lack of such compensation, as discussed in Section 3.2.1. The exaggerated topography can potentially be reduced by applying the topographic correction factor as described in Section 3.2.2. However, in the experiments of Calignano et al. (2015) the authors scale densities (not density contrasts), which means that Eq. (27) should be used and a topographic correction should not be applied. An explanation for the extreme topography in their models of 24–26 km should thus be sought elsewhere. Martinod et al. (2013), however, do scale density contrasts (not densities), so a topographic correction is required. Martinod et al. (2013) used a sub-lithospheric upper mantle density of ρ_{SLUM} = 1416–1434 kg/m^3 and a density contrast ratio of ~0.44. With ρ_{SLUM} = 3200–3300 kg/m^3 in nature, then C_{Topo} = ~0.194, and so their scaled topography would reduce from −20 km (backarc) and 40 km (leading edge overriding plate) to approximately −4 km and 8 km, respectively. The positive topography is still a factor of ~2 too high, but evidently more realistic than its uncorrected counterpart. As for the −4 km topography of the backarc region, there appears to be no natural counterpart in the Andes, whose backarc region is a few hundred meters above sea level.

The possible explanation for the extreme topography in Calignano et al. (2015) (about an order of magnitude too high) and the corrected topography in Martinod et al. (2013) that is a factor of ~2 too high is that they result from the combined modelling approach, in which the externally applied velocity induces a force to the system that is too high compared to the internal buoyancy forces. Indeed, subduction models that use an internal approach generally appear to have lower topographies. For example, in Schellart (2008) internally-driven subduction models produced maximum topographies at the trench of approximately −2 to −1 mm, scaling directly to −12 to −6 km (using his length scale factor where 1 cm corresponds to 60 km). Using a topographic correction factor of C_{Topo} = ~0.44 (Eq. (22)), then these values reduce to approximately −5.3 to −2.6 km, which is comparable to trench depths (although somewhat on the low side) in nature.

As illustrated above with the two examples of exaggerated topography, comparison of scaled (and possibly corrected) topography in models with topography in nature can be used to gauge if, in an isostatically supported laboratory experiment (e.g. subduction or lithospheric shortening) that uses the combined approach, the applied external forces are properly scaled or not. In case the topography is too high, then it is very possible that the externally applied forces are too high when compared to the buoyancy forces internal to the system. As such, we argue that, when using the combined approach, externally applied forces need to be quantified systematically and compared with buoyancy forces internal to the system to find out how these forces compare with respect to one another and to nature.

3.2.4. Absence of erosion

Most analogue models do not include processes of erosion, although there are a number of studies where such erosion is implemented, either through removing material from the top (e.g. Mugnier et al., 1997; Casas et al., 2001; Konstantinovskaia and Malavieille, 2005; Le Guerroué and Cobbold, 2006) by using, for example, a vacuum cleaner, or through the precipitation of fine water droplets, which can coalesce to form small streams, channels and rivers that generally erode material from the highest parts of the model and cause sedimentation in the lowest parts of the model (e.g. Graveleau et al., 2008; Strak et al., 2011; Graveleau et al., 2015). The absence of erosion in an analogue model causes the topography and maximum elevation to be higher than when erosion would be present. For experiments that are not isostatically supported, there is a one-to-one correlation between erosion and reduction in maximum elevation, where, for example, 1 mm of erosion from the topography would result in a 1 mm reduction in maximum elevation. For experiments that are isostatically supported, isostasy causes partial rebound of the surface during erosion. Consider again a crustal layer resting on top of a homogeneous upper mantle layer in isostatic equilibrium as shown in Fig. 2. Then, using equation (20), it can be easily shown that the change in elevation Δh of the topography of the crustal layer due to erosion z of the crustal layer is:

$$\Delta h = -z\frac{(\rho_{UM} - \rho_{CC})}{\rho_{UM}} \tag{28}$$

For example, in a laboratory experiment with 1 mm of erosion of the crust, assuming ρ_{UM} = 1400 kg/m^3 and ρ_{CC} = 1200 kg/m^3, the change in topography Δh is only −0.14 mm. Considering this isostatic rebound effect, it is unlikely that the extreme topography of the isostatically supported experiments as discussed in Section 3.2.3 can be explained by the lack of erosion. As such, we conclude again that for those experiments, the exaggerated topography likely originates from the externally imposed velocity boundary conditions that impose forces on the experimental layers that are too high when compared to the internal buoyancy forces of these experiments and too high when scaled to values in nature.

3.2.5. Other factors that could affect surface topography

There are other processes that affect surface topography in laboratory models but do not affect surface topography in nature (or only in a negligible way), because they are irrelevant at the length scale of the natural prototype. These include surface tension and shear zone dilatation. Surface tension is particularly evident in laboratory models that use only fluids and a free top surface boundary condition, and has been discussed for subduction experiments (Jacoby, 1976; Schellart, 2008). For example, the effects of surface tension have been observed in laboratory subduction models at the material boundary between silicone (the model plate), syrup (the model ambient mantle) and air (Schellart, 2008). From such observations it is evident, however, that surface tension will generally only affect the model surface topography on a very short horizontal

length scale of maximally several mm across the material boundary, while in other locations surface topography is not affected.

In laboratory models the brittle upper crust is often simulated with granular material. When a shear zone develops in the granular material, shear zone dilatation takes place, which is generally much more pronounced than dilatation in natural shear zones (e.g. Horsfield, 1977; Mandl, 1988). In addition, the scaled values of laboratory granular shear zone width are generally much larger than those in nature (see Section 4.1). The high reduction in density of the sheared granular material, in combination with the relatively large width of the shear zone causes laboratory shear zones to produce a more pronounced topographic signal than what would be expected in the natural prototype. As with surface tension, granular shear zone dilatation will generally only affect the model surface topography on a relatively short horizontal length scale (comparable with the width of the shear zone), while in other locations surface topography is not affected. The affected area will generally be of the order of several mm across the shear zone, in particular in case the shear zone is steep (dipping 60–90°) as with strike-slip, normal and high-angle reverse faults. In case of thrust faults (dipping 30° or less), it is evident that the surface topography will be affected over a larger area (i.e. the area that lies directly above the thrust fault).

3.3. Scaling of subduction models

In laboratory-based subduction modelling, as in other analogue modelling, geometric, kinematic and dynamic similarity are essential. To obtain dynamic similarity it is important that the driving forces and resistive forces are properly scaled. Depending on if one scales for densities or density contrasts, one can use Eqs. (8) and (9) or Eqs. (13) and (14) to scale stresses and forces. The most important driving force in most subduction settings is the negative buoyancy force of the slab, and so in many subduction simulations it is justified to use an internal (buoyancy-driven) modelling approach. There are subduction settings where external far-field tectonic forces also play a role, and so a combined approach would be justified. However, in order to satisfy dynamic similarity, it is essential that the externally-imposed force is quantified and properly scaled with respect to the internal buoyancy forces of the system. Unfortunately, this is generally never done in analogue subduction modelling (see Section 2.2 and Section 2.5). Laboratory experiments using a combined approach have been presented recently in which horizontal forces related to imposed velocity boundary conditions have been quantified (Boutelier and Cruden, 2013). Such an approach is a step in the right direction to allow for quantitative scaling of externally imposed forces.

The main resistive forces in subduction systems (and thus the main energy sinks) are exerted by the sub-lithospheric upper mantle, the tectonic plates and the subduction zone interface. To properly scale the distribution of the resistive forces in the experimental system, the ratios of the effective viscosities of the subducting plate (η_{SP}), overriding plate (η_{OP}) and subduction interface (η_{SI}) with respect to the sub-lithospheric upper mantle (η_{SLUM}), need to be comparable in model and nature:

$$\frac{\eta^m_{SP}}{\eta^m_{SLUM}} = \frac{\eta^p_{SP}}{\eta^p_{SLUM}} \tag{29a}$$

$$\frac{\eta^m_{OP}}{\eta^m_{SLUM}} = \frac{\eta^p_{OP}}{\eta^p_{SLUM}} \tag{29b}$$

$$\frac{\eta^m_{SI}}{\eta^m_{SLUM}} = \frac{\eta^p_{SI}}{\eta^p_{SLUM}} \tag{29c}$$

Laboratory subduction modelling studies have so far used a wide variety of viscosity ratios between the subducting plate and ambient mantle varying some 5 orders of magnitude, from relatively low values, i.e. of the order 2×10^2 (Schellart, 2004a,b; Meyer and Schellart, 2013; Chen et al., 2015b), 6×10^2 (Mériaux et al., 2015a,b) and $3.5–10 \times 10^2$ (Funiciello et al., 2003), to intermediate values, i.e. of the order 1.5×10^3 (Bajolet et al., 2013), 6×10^3 (Guillaume et al., 2009), 1.2×10^4 (Heuret et al., 2007) and 1.5×10^4 (Martinod et al., 2013), to relatively high values, i.e. of the order $10^4–10^5$ (Funiciello et al., 2006) and $10^6–10^7$ (e.g. Shemenda, 1992, 1993; Chemenda et al., 1995, 1996, 2000; Boutelier et al., 2003; Boutelier and Chemenda, 2008; Boutelier and Cruden, 2008, 2013). Using different lines of evidence, a variety of works imply that in nature the effective viscosity ratio η_{SP}/η_{SLUM} is in the range 50–500 (e.g. Moresi and Gurnis, 1996; Billen et al., 2003; Schellart, 2008; Funiciello et al., 2008; Loiselet et al., 2009; Ribe, 2010; Li and Ribe, 2012).

The highest effective viscosity ratios in subduction models have generally been obtained for subduction models that use water as an analogue for the sub-lithospheric mantle (e.g. Shemenda, 1992, 1993; Chemenda et al., 1995, 1996, 2000; Boutelier et al., 2003; Boutelier and Chemenda, 2008; Boutelier and Cruden, 2008, 2013). Although water can provide isostatic support to the overlying plates, it provides negligible shear and normal tractions to the plates and slab. Furthermore, it causes subduction in such experiments to generally occur at a very short timescale and experimental velocities of the sinking slab to be relatively high, of the order of mm/s to cm/s, and thus inertial forces in such experiments are not negligible. This brings us to another important part of laboratory subduction modelling, namely, that experiments need to be conducted at very low Reynolds number (Re). The Reynolds number is a non-dimensional number that represents the ratio of inertial forces to viscous forces and is defined as:

$$Re = \frac{\rho d v}{\eta} \tag{30}$$

where ρ is the density of the ambient fluid (e.g. sub-lithospheric upper mantle), d is the characteristic length scale of the sinking object (e.g. slab for subduction modelling, which can be its length, width or thickness), v is the characteristic velocity of the object (for the slab this can be its subduction velocity, rollback velocity or downdip sinking velocity), and η is the viscosity of the ambient fluid. The Reynolds number indicates in which flow regime a particular system is. For sinking slabs in nature Re is extremely low ($Re \ll 1$), and so one can expect flow in the ambient mantle to be in the laminar symmetrical flow regime. For example, with $\rho = 3300$ kg/m^3, $d = 600$ km, $v = 5$ cm/yr and $\eta = 10^{20}$ Pa s, then $Re = 3 \times 10^{-20}$. Such a low number cannot be achieved in laboratory experiments, but this is not required. What is required is that in the experiment the condition $Re \ll 1$ is met. In that case, the experiment is conducted in the same (laminar symmetrical) flow regime for the sub-lithospheric mantle (Schellart, 2008), without eddy formation in the wake of the object (Hudson and Dennis, 1985) (e.g. slab) nor any turbulence.

4. Analogue modelling materials

Scaled laboratory models make use of analogue materials to simulate the physical behaviour of natural rocks whose tectonically-induced deformation strongly depends on rheology. As a consequence, the choice of analogue materials should be addressed carefully according to rheology-dependent scaling relationships between the model and the natural prototype, which makes scaling and the selection of analogue materials intimately related. Observation-based disciplines such as seismology and geochemistry have greatly improved our knowledge of the compo-

sitional and physical layering of the Earth. The resulting rheological stratification imposes strong conditions on how one should build a rheologically scaled analogue model. If the purpose of such model is to simulate a geodynamic process that occurs at a scale from the Earth's surface to the core-mantle boundary, then the choice of the analogue materials should reflect the observed rheological layering. Such rheological layering can be complex, for example if one considers a model of a young stable continental lithosphere overlying a sub-lithospheric mantle, which consist of (1) a brittle material to simulate the upper crust, (2) a ductile material to simulate the lower crust, (3) a strong brittle or ductile material to simulate the uppermost lithospheric mantle, (4) a ductile material to simulate the lowermost lithospheric mantle (e.g. Davy and Cobbold, 1991), and (5) a viscous upper and lower mantle with or without a viscosity jump at the 660 km discontinuity. Increasingly sophisticated models could also include lateral viscosity variations in the mantle, through, for example, incorporating lateral temperature gradients and temperature-dependent viscosities.

Historically, the first analogue models were focused on upper crustal deformation in sedimentary layers and used fabric pieces of different composition and thickness to simulate strength contrast (e.g. Hall, 1815; Lyell, 1871; Meunier, 1904). The use of natural materials such as clays, soil, gypsum, and sand was quickly recognised as effective in experiments since it allowed the simulation of folding concurrently with faulting and fracturing (e.g. Hall, 1815; Favre, 1878a,b; Daubre, 1879; Schardt, 1884; Cadell, 1889; Willis, 1893; Meunier, 1904). A breakthrough in analogue modelling occurred with the advent of the scaling theory (Hubbert, 1937), which indicated that only those materials could be used in analogue modelling that would ensure proper geometric, kinematic, and dynamic similarity between model and nature (see Section 3). A direct implication of the scaling theory is the suitability of materials such as granular materials to simulate the brittle upper crust, since they both deform according to the Mohr-Coulomb failure criterion, which allows one to scale down stresses and properties such as cohesion using the dynamic scaling relationship (Hubbert, 1951).

4.1. Brittle materials

The dominant brittle materials that are used in analogue modelling of small-scale and large-scale geodynamic processes are granular materials. Through the development of the scaling theory, Hubbert (1937) showed that granular materials are appropriate to simulate the brittle upper crust. Similar to brittle crustal rocks, granular materials deform according to the Mohr-Coulomb failure criterion (Coulomb, 1773), with shear stress increasing approximately linearly with normal stress (Mandl et al., 1977; Krantz, 1991; Schellart, 2000; Lohrmann et al., 2003) as follows:

$$\tau = \mu\sigma_n + C_0 \tag{31}$$

where τ and σ_n are the shear (tangential) stress and normal stress applied to the fault plane, respectively, C_0 is the apparent cohesion and μ the coefficient of internal friction (with $\mu = \tan(\varphi)$, φ is the angle of internal friction) of the sheared material. Uniaxial compressive tests and shear tests show that brittle crustal rocks have an angle of friction ranging between ~25–45° and a cohesion ranging between ~5–180 MPa, depending on rock type (e.g. Lama and Vutukuri, 1978; Schellart, 2000 and references therein). Shear tests on granular materials such as dry glass microspheres and quartz sand indicate a similar angle of internal friction ranging between ~27–42° and an apparent cohesion of ~50–250 Pa (McClay, 1990; Cobbold and Castro, 1999; Schellart, 2000; Lohrmann et al., 2003; Hampel et al., 2004; Panien et al., 2006; Schreurs et al., 2006; Hoth et al., 2007). This ensures proper dynamic similarity between nature and model with cohesion scaling down in the same proportion as stresses following Eq. (8) or Eq. (13) (Horsfield, 1977; Davy and Cobbold, 1988; Cobbold and Jackson, 1992). Also, as a result, sand produces shear zones similar to natural faults to the first order, with the development of thrust, normal and strike-slip faults, because the control of principal stresses on dip and dip direction of shear zones in granular materials is similar as for the Andersonian faults (Anderson, 1905) observed in nature (e.g. Krantz, 1991). Furthermore, shear stress variation with progressive shear strain for granular materials is similar as for deformed rock samples (Lohrmann et al., 2003 and references therein). Shear zones in analogue models show a phase of strain hardening before failure and a consecutive phase of strain softening before reaching a state of constant shear strength allowing the shear zone to remain active (stable-dynamic shear strength). The phase of strain hardening preceding failure is due to compaction and associated bulk density increase in the shear zone. The following phase of strain softening results from decompaction in the shear zone and associated volume increase (dilatancy) (Mandl et al., 1977; Panien et al., 2006).

With the progressive increase of analogue modelling studies focusing on upper crustal deformation, the diversity of granular materials used in such modelling studies has risen as well, and consequently the range of physical and mechanical properties has widened. This increased variety has enlarged the range in density, size, and shape of the granular materials, thereby impacting on compaction, friction angle, and apparent cohesion, as shown by shear test measurements (Mandl et al., 1977; Krantz, 1991; Schellart, 2000; Lohrmann et al., 2003; Rossi and Storti, 2003; Panien et al., 2006; Gomes, 2013). Consequently, making use of various granular materials in analogue modelling can be practical since they can serve different purposes depending on their physical and mechanical characteristics (Table 1). It should be noted that dry granular materials have been used not only to simulate the brittle upper crust but also the brittle upper lithospheric mantle. Dry granular materials commonly used in analogue modelling include quartz sand (see reviews by Cobbold and Castro, 1999; Graveleau et al., 2011; Dooley and Schreurs, 2012), feldspar powder (e.g. Sokoutis et al., 2005; Corti and Manetti, 2006; Corti, 2008; Luth et al., 2013a; Calignano et al., 2015), glass microspheres or microbeads (e.g. Colletta et al., 1991; Leturmy et al., 2000; Schellart et al., 2002a,b, 2003; Rossi and Storti, 2003; Koyi and Vendeville, 2003; Konstantinovskaia and Malavieille, 2005; Hoth et al., 2007; Autin et al., 2010; Malavieille, 2010), silica powder (e.g. Colletta et al., 1991; Konstantinovskaia and Malavieille, 2005; Galland et al., 2006; Bonnet et al., 2007), clay powder (e.g. McClay, 1990; Krantz, 1991; Gartrell, 1997; Sherlock and Evans, 2001; Hampel et al., 2004), mica flakes (e.g. McClay, 1990; Storti et al., 2000; Gomes, 2013), and ethyl cellulose powder (e.g. Davy and Cobbold, 1988, 1991; Ratschbacher et al., 1991; Cobbold and Jackson, 1992; Faccenna et al., 1996; Cagnard et al., 2006; Marques and Cobbold, 2006; Schueller and Davy, 2008; Bajolet et al., 2015). Other dry granular materials include aluminium microspheres (e.g. Rossi and Storti, 2003; Autin et al., 2010), walnut shells (e.g. Cruz et al., 2008), hollow microspheres (Dooley et al., 2009), and sugar powder (e.g. Keep, 2000; Moore et al., 2005a,b; Zhang et al., 2006).

Analogue modellers have simulated brittle deformation in sedimentary basins and accretionary wedges. Construction of a layered sequence of granular materials with a different coefficient of internal friction and apparent cohesion has allowed modellers to study faulting in a sedimentary sequence consisting of alternating rock strength such as in the case of interbedded limestones and clays (e.g. McClay, 1990), or layered sequences with weak detachment levels (e.g. McClay, 1990; Colletta et al., 1991; Leturmy et al., 2000; Storti et al., 1997, 2000; Koyi and Vendeville, 2003; Teixell and Koyi, 2003; Konstantinovskaia and Malavieille, 2005; Rossi and Storti, 2003; Hoth et al., 2007; Malavieille, 2010). It has also allowed

Table 1
A list of granular materials used in analogue modelling, with indication of peculiarity(ies) regarding their physical properties and associated purpose in laboratory models.

Granular material	Peculiarity	Purpose	References
Quartz sand	Φ and C consistent for dynamic scaling	Simulate the brittle upper crust	Krantz (1991) Cobbold and Castro (1999) Schellart (2000) Graveleau et al. (2011) Dooley and Schreurs (2012)
K-Feldspar powder	Φ and C consistent for dynamic scaling	Simulate the brittle upper crust	Sokoutis et al. (2005) Corti and Manetti (2006) Corti (2008) Luth et al. (2013a) Calignano et al. (2015)
Glass microbeads	Relatively low Φ and low C	Simulate weak detachment levels or brittle lithosphere	Krantz (1991) Colletta et al. (1991) Schellart (2000) Leturmy et al. (2000) Schellart et al. (2002a,b) Schellart et al. (2003) Koyi and Vendeville (2003) Konstantinovskaia and Malavieille (2005) Hoth et al. (2007) Malavieille (2010)
	X-ray attenuation different from sand	X-ray tomography	Colletta et al. (1991)
Silica powder	High C	Increase strength	Konstantinovskaia and Malavieille (2005) Galland et al. (2006) Bonnet et al. (2007)
	X-ray attenuation different from sand	X-ray tomography	Colletta et al. (1991)
Clay powder	Relatively high C	Increase strength	McClay (1990) Krantz (1991) Gartrell (1997) Hampel et al. (2004)
	Increase bulk modulus	Seismic reflection	Sherlock and Evans (2001)
Mica flakes	Low Φ, negligible C	Simulate weak detachment levels	McClay (1990) Storti et al. (2000)
Sand + Mica flakes	Increase duration of plastic deformation before failure	Simulate more distributed deformation	Gomes (2013)
Ethyl cellulose powder (added to quartz sand)	Decreases bulk density	Prevent sand from sinking into viscous materials placed underneath	Davy and Cobbold (1988) Davy and Cobbold (1991) Ratschbacher et al. (1991) Faccenna et al. (1996) Cagnard et al. (2006) Marques and Cobbold (2006) Schueller and Davy (2008) Bajolet et al. (2015)
Glass and aluminium microspheres	Relatively low Φ, low C, and low density	Simulate weak detachment levels or brittle lithosphere	Schellart (2000) Rossi and Storti (2003)
		Simulate the brittle upper crust and upper lithospheric mantle	Autin et al. (2010)
Walnut shells	Relatively low density and low abrasion	Allow to increase height of layer and avoid scratching sidewalls	Cruz et al. (2008)
Caster sugar	Relatively low density but high Φ and C	Simulate the brittle upper crust	Schellart (2000) Moore et al. (2005a,b)
Sugar powder (added to quartz sand)	Decreases bulk density	Simulate the brittle upper crust and upper lithospheric mantle	Keep (2000) Zhang et al. (2006)

Φ is the angle of internal friction and C is the cohesion of the granular materials.

investigations of fault refraction (Schöpfer et al., 2007). Besides dry granular materials, wet clay has also been used to simulate the brittle upper crust, such as in strike-slip experiments (Dooley and Schreurs, 2012 and references therein). However, despite having an angle of internal friction similar as sand, cohesion of wet clay is dependent on water content (Eisenstadt and Sims, 2005) and is generally poorly constrained (Dooley and Schreurs, 2012), making it difficult to dynamically scale laboratory experiments that use clay. Other wet granular materials are also commonly used to investigate geomorphologic problems (Graveleau et al., 2011 and references therein). Their apparent cohesion is generally higher than dry quartz sand (van Mechelen, 2004; Richefeu et al., 2006; Graveleau et al., 2011,2015; Strak et al., 2011) and therefore the length scale needs to be adjusted accordingly, considering that cohesion scales as stresses following Eq. (8) or Eq. (13) (Graveleau and Dominguez, 2008; Graveleau et al., 2011, 2015; Strak et al., 2011).

Despite the striking resemblance between the features related to brittle deformation in the laboratory and those observed in nature, the similarity between shear zones developing in granular materials and natural faults is imperfect. In granular analogue materials, the width of shear zones during dilatancy increases with mean grain size (e.g. McClay, 1990) and is ~11–16 times the mean grain size (Panien et al., 2006). It is consequently often disproportionate to the thickness of fault gouges in nature (Horsfield, 1977; Mandl, 1988), and indicates that dilatancy of shear zones in granular materials does not scale to natural faulting processes occurring in fault breccias (Krantz, 1991). Therefore, if the purpose is to attain a high degree of structural detail, it appears most appropriate to use granular materials with a small grain size (Rossi and Storti, 2003). Furthermore, caution should be taken when considering friction and cohesion of natural faults since they can be affected by processes that are not simulated in the laboratory, such as fault sealing, formation of anisotropic fabric (Lohrmann et al., 2003), and fluid pressure. In addition, the strength of undeformed brittle materials is generally higher than when reactivation occurs (Brace and Byerlee, 1966; Byerlee, 1978; Paterson, 1978). Thus, the bulk strength and apparent cohesion of the pre-fractured upper continental crust should be smaller than the quasi-intact oceanic crust (Schellart, 2000). Moreover, rock shear tests and uniaxial compressive tests show that cohesion of natural rocks depends on composition and varies by one order of magnitude. For these reasons, the modeller should carefully consider which analogue granular material is most suitable to represent the rock prototype in nature. Nevertheless, shear zones in granular materials are weaker than the surrounding (undeformed) granular material, which thereby mimics the behaviour of brittle rocks in nature (Krantz, 1991).

Schreurs et al. (2006) showed that differences in analogue granular materials induce variations in the resulting geometries and

evolution of structures such as thrust belts. This relates to the fact that different granular materials can have different values for friction angle and cohesion. Indeed, both the angle of internal friction and the apparent cohesion are dependent on grain shape (Schellart, 2000) and handling technique (Mandl et al., 1977; Krantz, 1991; Lohrmann et al., 2003). Pouring and sieving of dry granular materials produce different bulk densities, which thereby affect the coefficient of friction of the material (Krantz, 1991). Again, this indicates that care should be taken when choosing a granular analogue material to simulate the brittle upper crust, and when setting up the experiment.

4.2. Materials with linear viscous, non-linear viscous, visco-plastic and complex ductile rheologies

A large variety of linear viscous, non-linear viscous, visco-plastic and complex ductile rheologies have been used in analogue modelling (Table 2). The most commonly used linear viscous (Newtonian) rheologies include glucose syrup, corn syrup and golden syrup (dynamic shear viscosity $\eta \approx 10^1$–10^3 Pa s, at room temperature), honey ($\eta \approx 10^0$–10^2 Pa s), sucrose or sugar solution ($\eta \approx 10^1$–10^2 Pa s), water ($\eta \approx 10^{-3}$ Pa s), and silicone putty ($\eta \approx 10^3$–10^5 Pa s) (e.g. Weijermars, 1986; Kincaid and Olson, 1987; Davy and Cobbold, 1991; Schellart, 2011). The low-viscosity materials such as sucrose or sugar solution (e.g. Kincaid and Olson, 1987; Davy and Cobbold, 1991), glucose syrup (e.g. Ratschbacher et al., 1991; Faccenna et al., 1999; Schellart, 2004a; Duarte et al., 2013), honey (e.g. Hatzfeld et al., 1997; Keep, 2003; Funiciello et al., 2003) and water (e.g. Jacoby, 1973; Shemenda, 1992, 1993; Chemenda et al., 1995, 1996, 2000; Boutelier et al., 2003; Boutelier and Cruden, 2013) have frequently been used to simulate the asthenosphere or sub-lithospheric mantle. In several cases corn syrup and glucose syrup have also been used to model sinking slabs (e.g. Griffiths et al., 1995; Guillou-Frottier et al., 1995). The higher viscosity silicone putties have mostly been used to simulate the ductile crust and ductile lithospheric mantle (e.g. Faugere and Brun, 1984; Davy and Cobbold, 1988, 1991; Faccenna et al., 1996, 1999; Schellart et al., 2002a,b; Schellart et al., 2003; Regard et al., 2003, 2005; Willingshofer and Sokoutis, 2009; Luth et al., 2013a), or the entire lithosphere (e.g. Funiciello et al., 2003, 2006; Schellart, 2004a, 2008; Bellahsen et al., 2005; Guillaume et al., 2009, 2010; Irvine and Schellart, 2012; Duarte et al., 2013; Martinod et al., 2013; Strak and Schellart, 2014; Chen et al., 2015a, 2015b).

A significant number of analogue models use visco-plastic and non-linear viscous materials, either exclusively or in combination with linear viscous materials. The most commonly used materials include hydrocarbon compositional systems, which are mixtures of solid hydrocarbons, powders and mineral oils (Shemenda, 1992, 1993; Chemenda et al., 1995, 2000; Boutelier et al., 2003; Boutelier and Cruden, 2013), plasticine (Tapponnier et al.,1982), wax (Brune and Ellis, 1997), petrolatum or petroleum jelly (e.g. Heuret et al., 2007; Bajolet et al., 2013) and paraffin oil-petrolatum mixtures (Duarte et al., 2013, 2014; Edwards et al., 2015). The latter two materials have in particular been used to coat the subduction zone interface in subduction experiments. Recently, visco-elastic foams have been used to simulate the seismic cycle on faults such as large strike-slip faults (Caniven et al., 2015).

In the last decade, a variety of materials with a composite rheology have been investigated that might be suitable to simulate the complex rheological behaviour of the crust, lithosphere and/or sub-lithospheric mantle. These materials in particular include gelatins and Carbopol hydrogels (Table 2). The rheology of the materials is dependent on several parameters, such as temperature, composition, concentration, pH (Carbopol) and strain rate (Carbopol, gelatins). The dependence on composition and concentration therefore allows one to adjust the rheology (Di Giuseppe et al., 2009, 2015). Gelatins have been mostly used to simulate intrusion processes in the upper crust because of their elastic-brittle rheology (see Di Giuseppe et al., 2009 and references therein; Kavanagh et al., 2015). More recently, the elastic behaviour of gelatins has also proven efficient to run laboratory models of the earthquake cycle along subduction megathrust faults (e.g. Corbi et al., 2013). Di Giuseppe et al. (2009) showed that gelatins have in fact visco-elastic-brittle properties and could be used to simulate the lithospheric rheological layering in presence of a vertical temperature gradient. However, the authors indicate a Reynolds number of $\sim 10^2$–10^3 in the sol state of gelatins. Such a high Reynolds number indicates that such materials are not suitable to simulate the sub-lithospheric mantle (see Section 3.3). Carbopol hydrogels have been recently used to study convection (Balmforth and Rust, 2009; Darbouli et al., 2013; Kebiche et al., 2014), thermal plumes (Davaille et al., 2013), and strain localisation in ductile strike-slip shear zones (Schrank et al., 2008). An advantage is that Carbopol promotes strain localisation with shear thinning, allowing one to better simulate natural shear zones (Schrank et al., 2008).

In case viscous materials are used in analogue experiments, scaling of viscosity should be performed. Natural viscous materials obey a power flow law linking stresses to strain rate $\dot{\varepsilon}$ (e.g. Weertman, 1978; Kirby, 1985), as follows:

$$\sigma^n = \dot{\varepsilon}\eta \tag{32}$$

where η is a material constant corresponding to the viscosity when $n = 1$. Stress exponent n depends on whether the flow occurs by diffusion creep, in which case $n \approx 1$ (linear flow law) and the material is linear viscous (Newtonian), or dislocation creep, in which case $n \approx 3$–5 (power flow law) and the material is non-linear viscous (e.g. Carter, 1976; Kirby and Kronenberg, 1987; Wang et al., 1994). Thus, to fulfil dynamic similarity with a correct balance of stresses between the model (superscript m) and the natural prototype (superscript p), the following equation can be written:

$$\frac{(\sigma^n)^m}{(\sigma^n)^p} = \frac{\dot{\varepsilon}^m \eta^m}{\dot{\varepsilon}^p \eta^p} \tag{33}$$

and considering that strain rate is a measure of a velocity over a length scale, we can rearrange to:

$$\frac{(\sigma^n)^m}{(\sigma^n)^p} = \frac{\eta^m t^p}{\eta^p t^m} \tag{34}$$

In Eq. (34), the stress exponent n should be similar for the model and the natural prototype to ensure dynamic similarity (Weijermars and Schmeling, 1986).

4.3. Rheological layering approaches

In analogue modelling, dynamic similarity requires rheological similarity, and thus rheological scaling of analogue models (Weijermars and Schmeling, 1986). To achieve rheological similarity in analogue models, three different rheological approaches have been used to simulate the rheological layering through the lithosphere and sub-lithospheric mantle (Fig. 3), and some of these approaches have also been used to represent rheological stratification in sedimentary basins. The scaling approach observed in the presence of a layering follows the scaling of densities or density contrasts, as reported in Section 3 (Eqs. (8) and (9) or Eqs. (13) and (14)). Furthermore, the analogue modeller has to consider scaling rheology in each layer. If a layer of granular material is present to simulate the brittle upper crust and, possibly, the upper lithospheric mantle, the model can thus be scaled for friction and cohesion in the granular layer(s). In case layers of viscous materials are present, scaling of viscosity should also be performed.

Table 2
A list of materials with linear viscous, non-linear viscous, visco-plastic and complex ductile rheologies used in analogue modelling, with indication of their rheological peculiarity(ies) and associated purpose in laboratory models.

Material	Rheological peculiarity(ies)	Purpose	References
Paraffin wax	Temperature-dependent apparent viscosity	Simulate the upper and lower crust	[R] Cobbold (1975) Jacoby (1976) [R] Neurath and Smith (1982) [R] Mancktelow (1988) Shemenda (1993) Chemenda et al. (1995) Brune and Ellis (1997) [R] Rossetti et al. (1999) Boutelier and Oncken (2011)
Paraffin oil	Newtonian with weak viscosity	Lubricant	Boutelier and Oncken (2011) [R] Duarte et al. (2014)
Petrolatum	Strain and strain-rate dependent	Lubricant	Corti et al. (2003) Cerca et al. (2004) Mart et al. (2005) Schreurs et al. (2006) Pastor-Galán et al. (2012) [R] Duarte et al. (2014)
Plasticine	Temperature-dependent, strain hardening, and strain-rate softening	Simulate dislocation creep in the lithosphere Simulate a layering if a temperature gradient is present	[R] McClay (1976) [R] Peltzer et al. (1984) [R] Weijermars (1986) [R]; Kobberger and Zulauf (1995) [R] Schöpfer and Zulauf (2002) [R] Zulauf and Zulauf (2004)
Silicone polymers	Newtonian at experimental (low) strain rates (10^{-5}-10^{-2} s^{-1})	Simulate long-term viscous deformation of lower crust and lowermost lithospheric mantle	[R] Dixon and Summers (1985, 1986); Dixon and Summers, 1985 [R] Weijermars (1986) [R] Weijermars and Schmeling (1986) Davy and Cobbold (1991) Nalpas and Brun (1993) Faccenna et al. (1999) Bonini et al. (2000) Koyi (2001) [R] ten Grotenhuis et al. (2002) Schrank et al. (2008)
Syrups and honey	Newtonian	Simulate diffusion creep in the sub-lithospheric mantle	Kincaid and Olson (1987) Davy and Cobbold (1988) Griffiths and Campbell (1990) Ratschbacher et al. (1991) Schellart et al. (2002a,b) Schellart et al. (2003) Funiciello et al. (2003, 2006) Schellart (2004a) Schellart (2008) Schellart (2010b) [R] Schellart (2011) Kerr and Mériaux (2004) Cruden et al. (2006) Schueller and Davy (2008) Mathieu et al. (2008) Guillaume et al. (2009, 2010) Davaille et al. (2011) Duarte et al. (2013) Chen et al. (2015a,b)
Water	Newtonian	Simulate diffusion creep in the sub-lithospheric mantle	Shemenda (1992, 1993) Chemenda et al. (1995, 1996, 2000) Boutelier et al. (2003) Boutelier and Oncken (2011) Boutelier and Cruden (2013)
Gelatins	Viscoelastic-brittle in their gel-state and viscous in their sol-state Rheology depends on temperature, composition, concentration, and strain rate	Simulate the viscoelastic-brittle behaviour of the crust/lithosphere Simulate a layering if a temperature gradient is present	[R] Di Giuseppe et al. (2009)
Carbopol® hydrogels	Viscoelastic-brittle strain softening and strain-rate softening Rheology depends on composition, concentration, pH, and temperature	Simulate the viscoelastic-brittle behaviour of the crust/lithosphere Simulate the convective mantle	Schrank et al. (2008) Balmforth and Rust (2009) Darbouli et al. (2013) Davaille et al. (2013) Kebiche et al. (2014) [R] Di Giuseppe et al. (2015)
Silicone polymers with granular fillers	Newtonian to visco-elastic with increasing filler content Strain-rate dependent	Simulate long-term viscous deformation of lithospheric plates at experimental low strain rates	[R] ten Grotenhuis et al. (2002) [R] Boutelier et al. (2008)
Silicone polymers mixed with plasticine	Viscoelastic-plastic strain hardening and strain-rate softening Temperature dependent	Viscoelastic-brittle behaviour of the crust/lithosphere Enhance ductile creep processes Simulate a layering if a temperature gradient is present	[R] Boutelier et al. (2008) Schrank et al. (2008)
Silicone polymers mixed with plastilina	Rheology depends on deformation history	Not yet used in analogue models	[R] ten Grotenhuis et al. (2002)
Plasticine mixed with granular fillers	Power-law exponent increases with filler content	Simulate dislocation creep in the lithosphere Simulate a layering if a temperature gradient is present	[R] Zulauf and Zulauf (2004)
Plasticine mixed with oil	Power-law exponent decreases with increasing oil content	Simulate dislocation creep in the lithosphere Simulate a layering if a temperature gradient is present	[R] Schöpfer and Zulauf (2002) [R] Zulauf et al. (2003) [R] Zulauf and Zulauf (2004)
Petrolatum-paraffin oil mixture	Strain and strain-rate dependent	Lubricant	[R] Duarte et al. (2014)

[R]indicates rheology studies.

4.3.1. *Isothermal brittle-viscous rheological layering*

The first approach on lithospheric layering consists of using materials with different rheologies and isothermal experimental conditions. Precursor models were dedicated to simulate crustal and lithospheric scale processes using for instance sand and silicone polymers for brittle and ductile behaviour, respectively (e.g. Faugere and Brun, 1984; Davy and Cobbold, 1988, 1991). Models from Davy and Cobbold (1988, 1991) were set to approximate predicted strength profiles of the lithosphere and asthenosphere. This approach has been widely used in modelling of large-scale tectonic processes such as lithospheric shortening, continental collision and fold and thrust belts (Davy and Cobbold, 1988, 1991; Cotton and Koyi, 2000; Keep, 2000; Martinod et al., 2000; Burg et al., 2002; Bonini et al., 2003; Sokoutis et al., 2005; Willingshofer et al., 2013; Cruden et al., 2006; Nilforoushan and Koyi, 2007; Schueller and Davy, 2008; Riller et al., 2010; Fernández-Lozano et al., 2011; Farzipour-Saein et al., 2013; Calignano et al., 2015), subduction (Faccenna et al., 1999; Willingshofer et al., 2013; Luth et al., 2013a), back-arc extension (Faccenna et al., 1996; Schellart et al., 2002a,b; Schellart et al., 2003), back-arc tectonic inversion

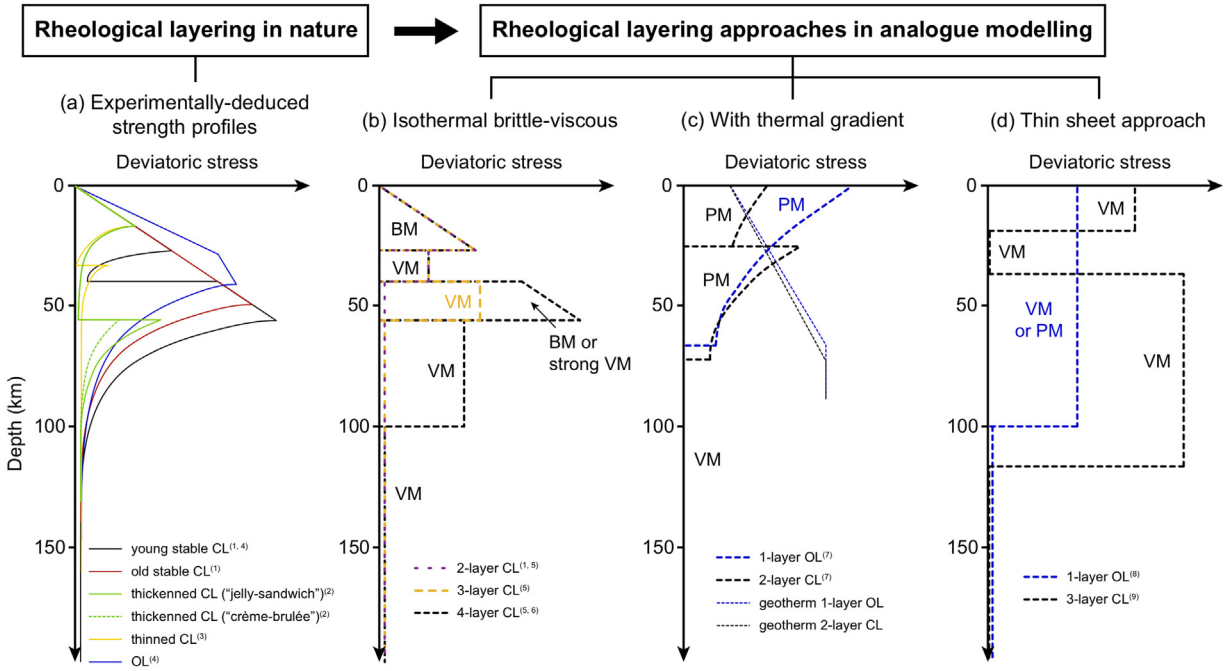

Fig. 3. Schematic strength profiles illustrating (a) how the rheological layering observed in nature is approximated using (b, c, d) three different approaches in analogue modelling of geological and geodynamic processes. (a) Examples of natural strength profiles deduced from experiments on rocks. (b, c, d) Examples of strength profiles used in analogue models. CL and OL indicate continental and oceanic lithosphere, respectively. BM, VM, and PM indicate brittle, viscous, and plastic materials, respectively. Numbers in superscript indicate the following references: (1) Brun, 1999; (2) Précigout and Gueydan, 2009; (3) Corti et al., 2003; (4) Kohlstedt et al., 1995; (5) Davy and Cobbold, 1991; Keep, 2000, 2003; Sokoutis et al., 2005; Willingshofer et al., 2013; (6) Autin et al., 2010; (7) Boutelier et al., 2003; (8) Tapponnier et al., 1982; Shemenda, 1992, 1993; Funiciello et al., 2003, 2006, 2008; Schellart, 2004a, 2008, 2010a; Bellahsen et al., 2005; Guillaume et al., 2009, 2010; Duarte et al., 2013; Strak and Schellart, 2014; Chen et al., 2015a, 2015b; (9) Göğüş et al., 2011.

(Munteanu et al., 2013), gravity spreading (Hatzfeld et al., 1997; Gautier et al., 1999; Martinod et al., 2000; Schellart and Lister, 2005), rifting (e.g. Vendeville et al., 1987; Allemand and Brun, 1991; Benes and Davy, 1996; Bonini et al., 1997; Lagabrielle et al., 2001; Bahroudi et al., 2003; Michon and Sokoutis, 2005; Autin et al., 2010), and core complexes (Malavieille, 1993; Brun et al., 1994). In this approach, materials used to model the viscous layers include silicone polymers and syrups (Table 2). It should be noted that brittle-viscous layering has also been simulated at the scale of the upper crust (e.g. thrust belts) or sedimentary cover (e.g. salt tectonics) by alternating layers of sand and silicone polymers (e.g. Merle and Guillier, 1989; Vendeville and Jackson, 1992; Casas et al., 2001; Bahroudi and Koyi, 2003; Luján et al., 2006; Storti et al., 2007; Bonini, 2007; Nilforoushan and Koyi, 2007; Koyi et al., 2008; Burliga et al., 2012). Models have also been built to simulate processes at the scale of layered sedimentary cover sequences, for example to study folding mechanisms in fold and thrust belts (e.g. Perrin et al., 2013). Silicone polymers are generally Newtonian viscous at low experimental strain rates and are used to simulate the lower crust and lithospheric mantle. As such, they only approximate the ductile behaviour of the prototype ductile layers that are generally thought to deform according to a power-law rheology and that may show strain localisation due to strain softening mechanisms. Furthermore, syrups such as honey and glucose syrup are also Newtonian viscous (Schellart, 2011) and can be considered as good analogues to simulate the viscous sub-lithospheric mantle, in particular if one assumes that diffusion creep is the dominant deformation mechanism (e.g. Trubitsyn, 2012).

4.3.2. *Rheological layering with thermal gradient*

In the second approach, the experimental model is subjected to a vertical temperature gradient and the lithosphere, and in some cases the sub-lithospheric mantle, are simulated with temperature dependent rheologies (Table 2) (e.g. Jacoby, 1976; Cobbold and Jackson, 1992; Brune and Ellis, 1997; Rossetti et al., 1999; Chemenda et al., 2000; Boutelier et al., 2003; Zulauf and Zulauf, 2004; Boutelier and Oncken, 2011). Thus, the models have the advantage of including the effect of thermal readjustments during model deformation. In addition, the layering of the lithosphere is caused by the applied temperature gradient (not by layers of different composition and rheology) because the rheology of the analogue material is highly sensitive to temperature. The resulting strength profile of the model lithosphere generally exhibits a relatively strong plastic part close to the surface and a weaker plastic part below, of which the strength decreases with depth (e.g. Boutelier and Oncken, 2011). In one group of models, experiments are conducted with only one material, such as paraffin wax (e.g. Jacoby, 1976; Brune and Ellis, 1997; Rossetti et al., 1999), while in another group of models materials with different compositions are used, such as solid hydrocarbon materials and water (e.g. Chemenda et al., 2000; Boutelier et al., 2003). Experiments using this modelling approach have studied subduction (Jacoby, 1976; Chemenda et al., 2000; Boutelier et al., 2003; Boutelier and Chemenda, 2008; Boutelier and Oncken, 2011; Boutelier and Cruden, 2013), orogenic wedges (Rossetti et al., 2000), and rifting (Brune and Ellis, 1997).

4.3.3. *Thin sheet approach*

In the third approach, the lithosphere rheology is approximated using a single viscous or plastic rheology under isothermal conditions, and an underlying viscous material can be present to simulate flow in the sub-lithospheric mantle and/or to provide isostatic support. No temperature gradient is applied, thus the rheological layering of the lithosphere is not simulated. Models using plastic material (plasticine) as analogue of the lithosphere have investigated indentation and extrusion tectonics (e.g. Tapponnier et al., 1982), and models using elasto-visco-plastic materials (solid hydrocarbon compositional systems) have been used to study

subduction and subduction initiation processes (e.g. Shemenda, 1992,1993). The plastic and elasto-visco-plastic analogue materials used in these experiments would generally simulate the lithosphere, and water was generally used to model the sub-lithospheric mantle (Table 2). Other modellers have used viscous silicone polymers to simulate the lithosphere (Table 2) in experiments investigating subduction (e.g. Funiciello et al., 2003, 2006, 2008; Schellart, 2004a, 2008, 2010a; Bellahsen et al., 2005; Guillaume et al., 2009, 2010; Duarte et al., 2013; Strak and Schellart, 2014; Chen et al., 2015a, 2015b), obduction (e.g. Agard et al., 2014; Edwards et al., 2015), delamination (e.g. Göğüş et al., 2011), and subducting plate-mantle plume interaction (Mériaux et al., 2015a, 2015b). Here, syrups such as honey, glucose syrup and sucrose solution are generally used to simulate the sub-lithospheric mantle. In some cases, however, syrups have also been used to model sinking slabs (Kincaid and Olson, 1987; Olson and Kincaid, 1991; Griffiths et al., 1995; Guillou-Frottier et al., 1995).

4.4. Analogue materials applied to subduction modelling

Subduction modelling in the laboratory started with pioneering models by Jacoby (1973), who used a rubber sheet and water to simulate the subducting lithospheric plate and the asthenosphere, respectively. Since then, analogue modellers have improved on the first subduction experiments from Jacoby (1973), using one of the three rheological approaches for analogue materials reported above (section 4.3).

In the first rheological approach, models considering the lithospheric layering with no imposed vertical temperature gradient have been done using sand mixed with ethyl cellulose or feldspar sand as analogue of the upper crust, silicone putty as analogue of the lower crust and lithospheric mantle, and glucose syrup or a mixture of glycerol and sodium polytungstate as analogue of the sub-lithospheric mantle (Faccenna et al., 1999; Regard et al., 2003; Luth et al., 2013a; Willingshofer et al., 2013). Here, an advantage is that models allow investigating the effect of the strength of the brittle and ductile layers on subduction evolution. In addition, the study of crustal and lithospheric deformation at the margin (e.g. by faulting) is possible. An obvious limitation of this rheological approach is that there is no thermal adjustment of the brittle and viscous layers during deformation, and thickening or thinning of layers only occurs through mechanical processes. Another limitation of experiments that use this rheological set-up is that they have so far only been conducted using the combined (external+internal) modelling approach (see Section 2.2). In these models, externally imposed forces have not been quantified nor compared to the internal buoyancy forces in the system. Thus, it is not known if these externally imposed forces are scaled with respect to the internal buoyancy forces and how these external forces scale to forces in nature.

In the second rheological approach, experiments imposing a vertical temperature gradient used paraffin wax (Jacoby, 1976) and solid hydrocarbon compositional mixtures (e.g. Chemenda et al., 2000; Boutelier et al., 2003; Boutelier and Oncken, 2011; Boutelier and Cruden, 2013) to simulate a temperature-dependent lithospheric strength profile. An advantage of these models is that they allow the experimenter to simulate the effect of temperature variation during model deformation, such as rheological weakening of a lithospheric plate that subducts into the hotter mantle or that is thinned due to back-arc extension and thus heated because of upwelling of hotter material. In addition, preparation of the experimental lithospheric plates can be done with a predefined geometry since the melted materials can be pored into a rigid mould, after which they can be left to cool to room temperature and then placed in the experimental tank as a strong rigid body that is easy to transport and handle. Another advantage is that by mixing the different base compounds with silicone polymers, granular fillers, and oil, the apparent viscosity and density of the materials can be adjusted according to the needs of the experimenter. Moreover, depending on the mixtures, materials can be produced that are sensitive to strain and strain-rate, and can be strain softening and strain-rate softening (shear thinning) (e.g. Boutelier and Oncken, 2011). Therefore, these materials can be seen as good rheological analogues of the ductile parts of the lithosphere that deform predominantly by dislocation creep (e.g. Hirth and Tullis, 1992). A limitation of most experiments using this rheological approach, however, is the use of water to model the sub-lithospheric mantle, as discussed in Section 3.3. Indeed, water has a viscosity that is too low by several orders of magnitude. As a consequence, viscous drag in the mantle is negligible, causing slab sinking velocities to be too high, thereby promoting inertial forces in the system that should be negligible in long-term natural subduction processes (e.g. Jacoby, 1976; Meyer and Schellart, 2013). Furthermore, the use of water causes the Reynolds number to be too high. For example, with a water density of 1000 kg/m^3, a typical length scale of 0.01–0.10 m, a typical subduction velocity of 10^{-3}–10^{-2} m/s and a water viscosity of 10^{-3} Pa s, $Re = 10^1$–10^3. This indicates that fluid motion in the model sub-lithospheric mantle, although possibly still laminar, is not in the symmetrical flow regime but in the asymmetrical flow regime with the formation of eddies and vortexes in the wake of the sinking object (Hudson and Dennis, 1985) (e.g. slab). As with the first rheological approach, experiments conducted with the second rheological approach have so far only used the combined approach (see Section 2.2).

In the third approach of models approximating the lithosphere with a single rheology using isothermal experimental conditions, a first set of studies has used plastic materials and water to simulate the lithosphere and sub-lithospheric mantle, respectively (Shemenda, 1992, 1993). The models have the same advantages as the experiments simulating a temperature-dependent lithospheric strength profile, except for the lack of a temperature gradient. The models also share the same disadvantages of using water for the asthenosphere and using the combined approach. A second set of studies has used viscous materials to simulate both the lithospheric plates and the sub-lithospheric mantle (Funiciello et al., 2003, 2006, 2008; Schellart, 2004a, 2008, 2010a,b; Bellahsen et al., 2005; Guillaume et al., 2009, 2010; Husson et al., 2012; Duarte et al., 2013; Meyer and Schellart, 2013; Strak and Schellart, 2014; Chen et al., 2015a, 2015b). This set of experiments uses a method similar to the thin viscous sheet approach used in numerical modelling (e.g. Bird and Piper, 1980; England and McKenzie, 1982; Vilotte et al., 1982). A disadvantage is the lack of simulation of a more realistic lithospheric strength profile by approximating the rheological behaviour of the lithosphere to its long-term viscous behaviour. Thus, this approach prevents the simulation of strain localisation in the lithosphere, which rather occurs by widespread, distributed deformation (Chen et al., 2015a, 2015b, 2016). However, these models have the advantage of allowing experiments to be fully dynamic (i.e. internal approach, see Section 2.3), thus allowing one to study the consequences of the different driving and resisting forces on the subduction process. In recent developments of this rheological approach, viscously layered plates have been constructed that have different effective viscosities, for example to study delamination of a viscous lithospheric mantle from a viscous continental crust (Göğüş et al., 2011), to study forearc obduction and continental subduction of a viscously layered continental lithosphere (Edwards et al., 2015), and to investigate subducting plate-overriding plate-mantle interaction and overriding plate deformation with a subducting plate that includes a weak visco-plastic crustal top layer (e.g. Duarte et al., 2013; Chen et al., 2015a,b).

5. Recording and quantification

5.1. What is recorded and what is quantified?

Recording pictures of laboratory models is crucial for qualitative and quantitative analysis. Commonly, analogue modellers document experiments by recording images at a constant rate, allowing the experimenter to visualise the evolution of the model, its state at a given stage, and also to perform manual or algorithmic-based post-processing to quantify the kinematics and topography (Sections 5.2, 5.3, and 5.4). The type of images that analogue modellers record depends on what information is required from the model to better constrain the natural prototype. In general, a surface view (map view) is used as it provides an element of direct comparison with the Earth's surface. In addition, one or more side views are frequently employed to give insights into model evolution at depth, using transparent glass or perspex sidewalls for the box containing the analogue materials. Side views can then be compared to geophysical data obtained for the natural prototype, such as data produced with seismic imaging. A limitation, however, is that side views generally provide the best view of the lateral edges of a model, which might not necessarily reflect precisely the geometry and processes occurring towards the centre of the model, except when the model geometry is laterally cylindrical and the boundary effects due to the sidewalls are limited. Additionally, a bottom view can be used to have access to processes occurring at depth below an opaque top layer. This can be useful, for instance, when motion occurs with a strong horizontal component at depth. Occasionally, analogue modellers also use oblique views in some specific circumstances, for instance to better visualise (qualitatively) topography or by using two oblique cameras in case of the stereoscopic particle image velocimetry technique (see section 5.3).

Because in some cases it is important to have a visual of the interior of the model, non intrusive techniques such as X-ray Computed Tomography (X-ray CT) scanning and seismic reflection have been developed in the lab to image internal structures at any time during the experiment. Analogue materials with different composition and/or contrasting bulk density can be used to visualise layering in models analysed with an X-ray CT scanner as their attenuation value differs (Colletta et al., 1991; Schreurs, 1994; Schreurs et al., 2001; Panien et al., 2006; Adam et al., 2008, 2013). X-ray CT scanning moreover allows one to visualise structures such as shear zones in granular materials as the density of shear zones is reduced during dilatancy (e.g. Panien et al., 2006). The resulting images produced with the X-ray CT scanning technique can be cross-sections of any direction as well as volumetric data (Adam et al., 2013). Seismic reflection is also applied in sandbox modelling and detects layers of granular material and shear zones (e.g. Sherlock and Evans, 2001; Krawczyk et al., 2013). Images generally produced in this case are cross-sectional seismic profiles. Another way of accessing the internal structures of a model is to slice it up at the end of an experiment. Analogue modellers can thus view features observed in serial cross-sections (e.g. McClay, 1990; Lu and Malavieille, 1994; Schreurs, 1994; Cotton and Koyi, 2000; Sokoutis et al., 2005; Graveleau et al., 2015), and then eventually digitise them to visualise their geometry in 3-D space using geomodelling software such as goCad (e.g. Konstantinovskaya et al., 2009; Ferrer et al., 2014). However, this method is applicable only at the end of the experiments and offers limited insights into internal processes occurring during model evolution.

From the different types of imaging techniques reported above, one can quantify various parameters such as (1) lengths and shapes to study the dimension and form of simulated geological features, (2) timescales that characterise the specific duration of modelled geological processes, (3) kinematics through manual-based or algorithmic-based post-processing, (4) and topography through the computation of digital elevation models. Below we discuss the main techniques of acquisition that have been developed to investigate kinematics and topography in analogue modelling, with applications to subduction experiments. The reader is also referred to Graveleau et al. (2012) for recording and quantification in accretionary wedge experiments.

5.2. Kinematic measurements with manual-based post-processing

Kinematic measurements are useful to obtain values of displacements, velocities, and deformation, and to study how these values evolve in time, thus giving insight into their past evolution in nature. Quantifying motion and deformation in models requires the use of passive markers that can be tracked in successive pictures. The first methods employed to study the kinematics in analogue modelling were done by drawing reference marks such as bands (Tapponnier et al., 1982), lines (e.g. Davy and Cobbold, 1991; Michon and Sokoutis, 2005; Rosas et al., 2015), grids (e.g. Davy and Cobbold, 1988; Faccenna et al., 1996; Bonini et al., 1997; Schellart et al., 2002a,b; Bahroudi et al., 2003; Bellahsen et al., 2003; Fournier et al., 2004; Sokoutis et al., 2005; Cruden et al., 2006; Nilforoushan and Koyi, 2007; Koyi et al., 2008; Schueller and Davy, 2008; Dell'Ertole and Schellart, 2013) and circles (e.g. Marques and Cobbold, 2002), or by placing passive markers such as spheres on top and/or on the sides of the models (e.g. Martinod and Davy, 1994; Schellart, 2004a). Drawing marks on models has been done using ink, a transfer method (e.g. Cruden et al., 2006), by placing granular materials such as coloured sand (e.g. Cotton and Koyi, 2000; Fournier et al., 2004), or by scratching the model surface (Marques and Cobbold, 2002). In models where deformed granular materials are observed in cross-section, layers of different colour are generally used as an equivalent of initially horizontal sedimentary strata, and they can be tracked during deformation to evidence uplift, subsidence, and folding (e.g. Konstantinovskaia and Malavieille, 2005). Individual coloured sand grains have also been used to track particle trajectories in accretionary wedge experiments (e.g. Konstantinovskaia and Malavieille, 2005). In models using a material influx, injected fluids are often dyed to provide a contrast with the overburden material, thus giving opportunity to follow their motion (e.g. Griffiths et al., 1995; Kerr and Mériaux, 2004; Mériaux et al., 2015a,b). Additionally, it can be noted that some elements in models present a natural contrast with the surrounding material, making them usable as markers. Such elements can be the contours of a dark lithospheric plate made of silicone and iron powder in subduction experiments, which provide a good contrast with the surrounding transparent glucose syrup simulating the sub-lithospheric mantle (e.g. Schellart, 2004a).

By manually tracking passive tracers reported in the above paragraph, measuring displacements and velocities punctually in models is relatively simple, provided that the size of one pixel on the picture is known accurately. In subduction experiments, quantifying motion and velocity of the trench, trailing edge of the subducting plate and, when present, trailing edge of the overriding plate is common (e.g. Jacoby, 1973; Kincaid and Olson, 1987; Guillou-Frottier et al., 1995; Funiciello et al., 2003; Schellart, 2004a; Duarte et al., 2013; Chen et al., 2015a). When measuring displacements and velocities, data accuracy and precision depend on pixel resolution. Precision is generally of 1–2 pixels and accuracy can be optimised by adjusting the interval time over which the displacement is observed. The trajectory of spherical passive tracers has also been used to determine slab motion at depth (e.g. Schellart, 2004a, 2005). Furthermore, to study the pattern of the sub-lithospheric mantle flow, Schellart (2008, 2010b) manually tracked tiny air bubbles in the glucose syrup to visualise their trajectory over a relatively short time, revealing the poloidal and toroidal compo-

nents of mantle flow. To investigate the anisotropy due to flow in the sub-lithospheric mantle, the long-axis orientation of small cylinders has been used as an approximation of the olivine fast *a*-axis orientation (Buttles and Olson, 1998; Druken et al., 2011). Finally, in analogue modelling grids and circles can be used to infer displacements, velocities, and deformation of multiple points. For instance, from a deformed grid Davy and Cobbold (1988) estimated the area of large-scale zones deformed by lateral escape and continental thickening. Another example is the use of a square grid by Marques and Cobbold (2002) to map surficial displacements, and of horizontal circles to mark deformation as they evolve into strain ellipsoids. Boutelier and Cruden (2008) also used passive marker grids imprinted on top of the subducting and overriding plates in their models, and they deduced the horizontal displacements and strains manually. However, measuring displacements and velocities for a high number of locations using manual-based post-processing tools is difficult and time consuming, and the use of algorithmic-based post-processing is preferable. Similarly, using computer algorithms is more appropriate to quantify deformation in experiments.

5.3. Kinematic measurements with algorithmic-based post-processing

Using algorithmic-based post-processing techniques is nowadays widespread in analogue modelling to compute displacement fields, velocity fields, and strain fields. Algorithms have been used to compute displacement and strain fields from square grids and grids made of points (e.g. Bellahsen et al., 2003; Fournier et al., 2004; Duarte et al., 2013; Chen et al., 2015a, 2015b). Such algorithms include the software Dynel (Maerten and Maerten, 2006) used in subduction modelling by Bellahsen et al. (2003), and SSPX (Cardozo and Allmendinger, 2009) used in subduction experiments by Duarte et al. (2013) and Chen et al. (2015a, 2015b). Note that with such methods the deformation grid needs to be digitised beforehand (e.g. Fournier et al., 2004; Duarte et al., 2013). Alternatively, a Matlab script can be used to compute the displacement and strain fields from the corners of a square grid (Nilforoushan and Koyi, 2007). With such methods the spatial resolution is mostly determined by the resolution of the grid imprinted on the model, and therefore it is difficult to achieve high spatial resolution.

In the 2000s, geodynamic analogue modelling has started to use the Particle Image Velocimetry (PIV) technique to compute displacement fields from which velocity fields and strain fields are derived. This technique was first developed for fluid dynamic analysis (see reviews by Grant, 1997; Raffel et al., 2007) and then, amongst other disciplines, started to be used in geodynamic analogue modelling to study deformation in accretionary wedges (Hampel et al., 2004; Adam et al., 2005; see review by Graveleau et al., 2012 and references therein), subduction-induced mantle flow (e.g. Kincaid and Griffiths, 2003, 2004), and thermal convection (e.g. Davaille and Vatteville, 2005; Kumagai et al., 2007). The PIV technique compares photos of the model taken at a regular time interval, and automatically recognizes motion by tracking groups of particles randomly distributed or any textural pattern inherently present in an analogue material. Therefore the model needs to contain particles of which the colour or grey level (for monochrome images) contrasts with the bulk analogue material, but which move passively when the material is deformed. The particles providing contrast can be placed inside the analogue material, such as graphite powder in granular materials (Graveleau and Dominguez, 2008; Strak et al., 2011) or grains of various compositions naturally present in sand (e.g. Hampel et al., 2004; Adam et al., 2005), and particles illuminated by a light sheet or laser sheet in transparent glucose syrup (e.g. Kincaid and Griffiths, 2003, 2004; Strak and Schellart, 2014, 2016). Alternatively, the tracked particles can be sprinkled on top of the model for PIV analysis of the model surface (e.g. Boutelier and Oncken, 2011; Chen et al., 2016). A textural pattern such as observed with walnut shells and pores can also be detected, provided the pattern itself does not deform between two pictures (Cruz et al., 2008).

The method to track the displacement of patterns of particles in 2-D involves a cross-correlation technique. The technique uses an interrogation window, computes its spectral signature in a reference image (time t), and moves the interrogation window incrementally to find the equivalent spectral signature in an image taken at a later time step (t + dt). Using a digital Fourier transform (see details in Raffel et al., 2007), a correlation map is then produced of which the correlation peaks correspond to the most likely local displacement vectors (e.g. Adam et al., 2005). Note that other image correlation methods exist (see in Grant, 1997; Raffel et al., 2007). However, the cross correlation method reported above is the most used in geodynamic analogue modelling. The PIV technique conveniently produces a displacement field with vectors on each node of a grid of which the resolution depends on the size of the interrogation window (e.g. Raffel et al., 2007). It can provide sub-pixel (<0.1 pixel) correlation accuracy when the size of the interrogation window, the seeding density of particles, and the time lapse between two correlated images (controlling the displacement) are optimised. Moreover, it is possible to improve correlation accuracy to 0.03-0.2 pixel as well as data resolution using an overlap when the interrogation window is moved, and using multi-pass interrogation algorithms (Adam et al., 2005; Raffel et al., 2007). In addition, some commercial PIV equipment (e.g. LaVision, GmbH) comes with a textured calibration board that allows scaling and correcting the images through the creation of a mapping function (e.g. Adam et al., 2005).

It should be noted that in addition to the PIV technique, other techniques to compute displacements exist and have been used, such as the Particle Tracking Velocimetry (PTV), the Feature Tracking (FT), and the optical flow techniques. The PTV technique tracks individual tracers and is best suited for a low seeding density of particles (Raffel et al., 2007). Therefore, its displacement field resolution is less than when using the PIV technique. As the PTV technique, the FT technique tracks individual particles (e.g. Funiciello et al., 2006). However its image correlation method uses an interrogation window similarly as the PIV technique, thereby improving calculation accuracy in comparison to the PTV technique. Another technique called optical flow (e.g. Gibson, 1950; Horn and Schunck, 1981) can use a similar cross-correlation as the PIV and FT techniques (e.g. Bernard et al., 2007; Graveleau and Dominguez, 2008) but is based on a different tracking method, which estimates motion between two images using the brightness patterns (Horn and Schunck, 1981).

Despite the diversity of techniques to track particle motion and compute displacement fields, the PIV technique has been the most widely used in geodynamic analogue modelling (e.g. Kincaid and Griffiths, 2003, 2004; Hampel et al., 2004; Adam et al., 2005; Davaille and Vatteville, 2005; Hoth et al., 2006, 2007, 2008; Yamada et al., 2006; Kumagai et al., 2007; Nilforoushan and Koyi, 2007; Cruz et al., 2008; Schrank et al., 2008; Konstantinovskaya et al., 2009; Schrank and Cruden, 2010; Boutelier and Oncken, 2011; Leever et al., 2011; Boutelier and Cruden, 2013; Corbi et al., 2013; Luth et al., 2013b; Strak and Schellart, 2014; Kavanagh et al., 2015). Furthermore, an advantage of the technique is that it can compute the 3 components of the displacement field on a plane. The technique is called stereo PIV and makes use of two oblique cameras recording the same area (Hampel et al., 2004; Adam et al., 2005; Strak and Schellart, 2014) (Fig. 4). The stereo cross-correlation method builds on the cross-correlation used in the 2-D PIV technique. First, the two in-plane projections of the 3-D velocity vector are calculated independently for each stereoscopic camera. Then, the out of plane

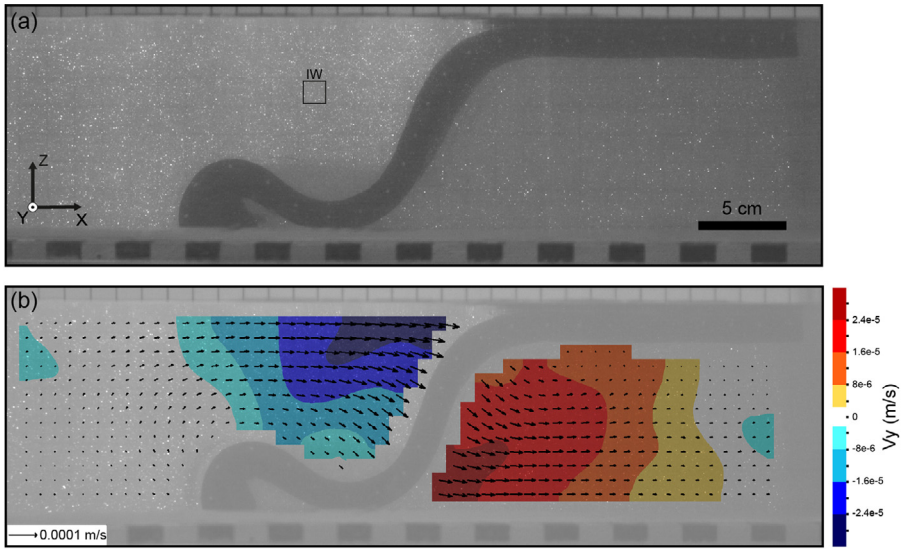

Fig. 4. An example of quantification of the velocity field in an analogue model of upper mantle subduction using the stereoscopic Particle Image Velocimetry (PIV) technique. (a) Side view photograph of the subduction model taken from one out of two stereoscopic cameras, illustrating the subducting plate and slab (in dark grey, made of a mix of silicone and iron powder) and the sub-lithospheric upper mantle fluid (light grey, made of glucose syrup, with white markers). A vertical laser sheet through the subduction zone and oriented perpendicular to the trench axis illuminates fluorescent particles mixed randomly in the transparent glucose syrup. IW indicates the interrogation window used for the stereo cross-correlation algorithm. Here a size of 64 pixels and an overlap of 50% were used during the stereo cross-correlation processing. The y-axis is represented with a dot and is oriented perpendicular to the x-z plane. (b) Resulting 3-D velocity field in a vertical plane through the subduction zone. Note that yellow, orange and red colours indicate velocity vectors coming out of the picture, and blue colours indicate velocity vectors going into the picture. A smoothing was used in postprocessing, which is justified as the glucose syrup is Newtonian. More information on the stereoscopic PIV technique and its usage in subduction modelling can be found in Strak and Schellart (2014).

component of the velocity vector is reconstructed from these two in-plane projections (Raffel et al., 2007). With the cameras placed in stereoscopic arrangement it is also possible to compute deformation on the surface affected by topographic changes (e.g. Adam et al., 2005). Another advantageous feature of the PIV technique is that it has proven efficient in calculating velocity fields at very high time resolution in laboratory models of the earthquake cycle (Rosenau et al., 2009; Corbi et al., 2013; Caniven et al., 2015). Furthermore, a recent method has been developed to compute the 3-D strain in a volume by combining X-ray CT scanning and digital volume techniques (Adam et al., 2013).

In subduction experiments, the PIV technique has been used to map streak patterns of the subduction-induced sub-lithospheric mantle flow in 2-D (Kincaid and Griffiths, 2003, 2004), the surficial velocity field and strain field in the overriding plate (Boutelier and Oncken, 2011; Boutelier and Cruden, 2013; Chen et al., 2016), the 2-D subduction-induced mantle flow velocity field (MacDougall et al., 2014), and the 3-D subduction-induced mantle flow velocity field in individual planes (Fig. 4) (Strak and Schellart, 2014, 2016; Chen et al., 2016). Funiciello et al. (2006) used a Feature Tracking (FT) technique to compute the subduction-induced mantle flow velocity field in 2-D.

5.4. Topography

In the last two decades, new techniques have allowed the construction of Digital Elevation Models (DEM) of the surface of geodynamic analogue models, enabling experimenters to study topography. Three different techniques are commonly used and they employ different acquisition devices. A first type of device widely used is the laser scanner (e.g. Martinod and Davy, 1994; Merle and Abidi, 1995; Rossetti et al., 2000; Cruden et al., 2006; Willingshofer and Sokoutis, 2009; Willingshofer et al., 2013; Autin et al., 2010; Fernández-Lozano et al., 2011; Husson et al., 2012; Luth et al., 2013a; Farzipour-Saein et al., 2013; Calignano et al., 2015). An advantage of the laser scanner is that it digitises directly topography without the need of recording pictures. However, a limitation is that digitalising topography for large model surfaces can be time consuming, and it often requires the model to be stopped. A second technique used to digitise topography is the fringe projection technique (Graveleau and Dominguez, 2008; Galland et al., 2009; Strak et al., 2011; Viaplana-Muzas et al., 2015). A laser interferometer projects fringes at the surface of the model and a camera records pictures simultaneously from above (Graveleau and Dominguez, 2008). A post-processing method then allows to compute the DEM using an unwrapping program. As with the laser scanner technique, this technique generally requires the modeller to stop the experiment during recording. A third technique employed to compute topography is by stereo photogrammetry (Donnadieu et al., 2003; Fischer and Keating, 2005; Schrank and Cruden, 2010; Riller et al., 2010). An advantage of this method is that it does not require any interruption of the model since it is based on pictures only. Another advantage is that this technique can be used in combination with a stereoscopic PIV technique. Therefore, it is possible to compute topography and 3-D velocity/strain fields at the same time (e.g. Adam et al., 2005). The three techniques share a very good 3-D resolution of 0.1-0.5 mm. In subduction experiments, the subduction-induced topography has been digitised using a laser scanner (Luth et al., 2013a; Husson et al., 2012; Willingshofer et al., 2013; Martinod et al., 2013).

6. Conclusions

In this review paper we have discussed the analogue modelling technique that has been used for some 200 years to investigate geological phenomena and geodynamic processes. From this work we draw the following conclusions:

1. Three fundamental modelling approaches can be defined in analogue modelling: (1) The external approach, (2) the combined (external+internal) approach, and (3) the internal approach (Fig. 1).

2. In the external approach, energy is added to the experimental system through the external application of a velocity, temperature

gradient or a material influx (or a combination thereof), and so the system is open. Furthermore, all deformation in the system is driven by the externally imposed condition. The external approach is mostly used to model microscale, mesoscale and upper crustal processes, which are generally driven by far-field tectonic forces rather than internal forces, thereby justifying the approach.

3. In the combined approach, energy is added to the experimental system through the external application of a velocity, temperature gradient or a material influx (or a combination thereof), and so the system is open. Here, deformation is partly driven by the externally imposed condition and partly by buoyancy forces internal to the system. The combined approach is mostly used to model upper crustal to mantle-scale processes.

4. In the internal approach, all deformation is driven by buoyancy forces internal to the system and so the system is closed and no energy is added during an experimental run. The internal approach is generally used to model upper crustal to mantle-scale processes.

5. The internal approach uses mostly linear viscous rheologies (e.g. silicone and syrup) sometimes in combination with brittle (e.g. granular materials) or visco-plastic (e.g. paraffin-petrolatum mixtures) rheologies. Both the combined and external approach use a larger variety of materials with different rheologies such as linear viscous, non-linear viscous, brittle, plastic, visco-plastic and visco-elasto-plastic rheologies (e.g. syrups, silicones, granular material, clay, plasticine, hydrocarbon composites, waxes, paraffin, petrolatum, gelatin).

6. The internal approach has the advantage that internal driving forces (buoyancy forces) can be accurately quantified and scaled, and can be compared to the internal resistive forces. The combined approach has the disadvantage that, in order to properly scale to nature, the externally imposed force or added energy needs to be quantified and compared to the internal buoyancy force or potential energy of the system. This is generally never done in experiments that use this approach, and so it is not known if these experiments are properly scaled with respect to nature.

7. The scaling theory requires that analogue models are geometrically, kinematically and dynamically similar to the natural prototype. Although experiments using the combined approach can be geometrically and kinematically similar, dynamic similarity cannot be guaranteed unless the externally imposed force or added energy is quantified and compared to the internal force or energy. One way to gauge if dynamic similarity is approximately achieved is through investigating the developing topography in the experiment.

8. Topography is often exaggerated in analogue models, which can be ascribed to: (1) The lack of isostatic compensation, which causes topography to be too high. (2) The lack of erosion, which causes topography to be too high, although the reduction of topography with erosion is reduced in isostatically supported experiments due to isostatic rebound (Eq. (28)). (3) The incorrect scaling of topography when density contrasts are scaled (rather than densities); Scaling of density contrasts requires an adjustment of the scaled topography by applying a topographic correction factor (Eq. (22)–(24)). (4) The incorrect scaling of externally imposed boundary conditions in isostatically supported experiments; When externally imposed forces are too high, this creates topography that is too high. Other processes that also affect surface topography in laboratory models include surface tension for fluids and shear zone dilatation in granular material. However, these will generally only affect the model surface topography on relatively short horizontal length scales of the order of several mm across material boundaries and shear zones, respectively.

9. A wide variety of analogue materials have been used in analogue modelling to simulate the different rheologies observed in nature. Analogue modellers employ materials with diverse rheologies such as viscous (e.g. syrups, silicones, water), brittle (e.g. granular materials such as sand, microspheres and sugar), plastic (e.g. plasticine), visco-plastic (e.g. paraffin, waxes, petrolatum) and visco-elasto-plastic (e.g. hydrocarbon compounds and gelatins).

10. One challenge is to simulate the rheological layering observed in nature, which can only be approximated. Three rheological layering approaches can be defined: (1) a first approach uses an isothermal brittle-viscous rheological layering with a lithosphere composed of 2, 3, or 4 layers; (2) a second approach employs a vertical thermal gradient and plastic-dominant materials to simulate a depth-dependent weakening; (3) a third approach uses the thin sheet approximation by simulating the long-term behaviour of the lithosphere as a bulk viscous material.

11. Models using an isothermal brittle-viscous rheological layering better approximate the lithospheric strength profile. However, they mostly use the external or combined approach and generally do not scale the external forces added to the system.

12. Models using the vertical thermal gradient have the advantage to better approximate the flow laws of ductile materials (lower crust and lower lithospheric mantle). However, they generally lack an upper brittle crust and an upper lithospheric mantle. They also generally use water to simulate the sub-lithospheric mantle, thereby leading to significant inertial forces.

13. Models using the thin sheet approach are the most simplistic regarding the approximation of the rheological layering. However, they mostly use the internal approach with its advantage that it allows for a fully dynamic evolution of the models.

Acknowledgments

We would like to thank Zhihao Chen and Joao Duarte for stimulating discussions on analogue modelling and scaling of analogue models. We would also like to thank reviewer Jacques Malavieille and an anonymous reviewer for providing constructive comments that have improved the contents of this review paper. This research was supported by a Future Fellowship (FT110100560) and a Discovery Grant (DP120102983) from the Australian Research Council awarded to W.P.S.

References

Abbassi, M.R., Mancktelow, N.S., 1992. Single layer buckle folding in non-linear materials-I Experimental study of fold development from an isolated initial perturbation. J. Struct. Geol. 14, 85–104.

Acocella, V., Cifelli, F., Funiciello, R., 2000. Analogue models of collapse calderas and resurgent domes. J. Volcanol. Geotherm. Res. 104, 81–96.

Adam, J., Urai, J.L., Wieneke, B., Oncken, O., Pfeiffer, K., Kukowski, N., Lohrmann, J., Hoth, S., van der Zee, W., Schmatz, J., 2005. Shear localisation and strain distribution during tectonic faulting—new insights from granular-flow experiments and high resolution optical image correlation techniques. J. Struct. Geol. 27, 283–301.

Adam, J., Schreurs, G., Klinkmüller, M., Wieneke, S., 2008. 2-D/3-D Strain localisation and fault simulation in analogue experiments: insights from X-ray computed tomography and tomographic image correlation. Bolletino di Geofisica 49, 21–22.

Adam, J., Klinkmüller, M., Schreurs, G., Wieneke, B., 2013. Quantitative 3D strain analysis in analogue experiments simulating tectonic deformation: integration of X-ray computed tomography and digital volume correlation techniques. J. Struct. Geol. 55, 127–149.

Agard, P., Zuo, X., Funiciello, F., Bellahsen, N., Faccenna, C., Savva, D., 2014. Obduction: why, how and where: clues from analog models. Earth Planet. Sci. Lett. 393, 132–145, http://dx.doi.org/10.1016/j.epsl.2014.02.021.

Allemand, P., Brun, J.P., 1991. Width of continental rifts and rheological layering of the lithosphere. Tectonophysics 188, 63–69.

Anderson, E.M., 1905. The dynamics of faulting. Trans. Edinburgh Geol. Soc. 8, 387–402.

Applegarth, L.J., James, M.R., van Wyk de Vries, B., Pinkerton, H., 2010. Influence of surface clinker on the crustal structures and dynamics of 'a' ā lava flows. J. Geophys. Res. 115, B07210, http://dx.doi.org/10.1029/2009JB006965.

Autin, J., Bellahsen, N., Husson, L., Beslier, M.-O., Leroy, S., d'Acremont, E., 2010. Analog models of oblique rifting in a cold lithosphere. Tectonics 29, http://dx.doi.org/10.1029/2010tc002671 (TC6016).

Bahroudi, A., Koyi, H.A., 2003. Effect of spatial distribution of Hormuz salt on deformation style in the Zagros fold and thrust belt: an analogue modelling approach. J. Geol. Soc. Lond. 160, 719–733.

Bahroudi, A., Koyi, H.A., Talbot, C.J., 2003. Effect of ductile and frictional décollements on style of extension. J. Struct. Geol. 25, 1401–1423.

Bajolet, F., Replumaz, A., Lainé, R., 2013. Orocline and syntaxes formation during subduction and collision. Tectonics 32, 1–18, http://dx.doi.org/10.1002/tect.20087.

Bajolet, F., Chardon, D., Martinod, J., Gapais, D., Kermarrec, J.J., 2015. Synconvergence flow inside and at the margin of orogenic plateaus: lithospheric-scale experimental approach. J. Geophys. Res. Solid Earth 120, 6634–6657.

Balmforth, N., Rust, A., 2009. Weakly nonlinear viscoplastic convection. J. Non-Newtonian Fluid Mech. 158, 36–45.

Bellahsen, N., Faccenna, C., Funiciello, F., Daniel, J.M., Jolivet, L., 2003. Why did Arabia separate from Africa? Insights from 3-D laboratory experiments. Earth Planet. Sci. Lett. 216, 365–381.

Bellahsen, N., Faccenna, C., Funiciello, F., 2005. Dynamics of subduction and plate motion in laboratory experiments: insights into the plate tectonics behavior of the Earth. J. Geophys. Res. 110, B01401, http://dx.doi.org/10.1029/2004JB0029999.

Benes, V., Davy, P., 1996. Modes of continental lithospheric extension: experimental verification of strain localization processes. Tectonophysics 254, 69–87.

Benn, K., Odonne, F., de Saint Blanquat, M., 1998. Pluton emplacement during transpression in brittle crust: new views from analogue experiments. Geology 26, 1079–1082.

Bercovici, D., Kelly, A., 1997. The non-linear initiation of diapirs and plume heads. Phys. Earth Planet. Inter. 101, 119–130.

Bernard, S., Avouac, J.P., Dominguez, S., Simoes, M., 2007. Kinematics of fault-related folding derived from a sandbox experiment. J. Geophys. Res. 112, http://dx.doi.org/10.1029/2005jb004149 (B03S12).

Billen, M., Gurnis, M., Simons, M., 2003. Multiscale dynamics of the Tonga-Kermadec subduction zone. Geophys. J. Int. 153, 359–388.

Bird, P., Piper, K., 1980. Plane-stress finite-element models of tectonic flow in southern California. Phys. Earth Planet. Interiors 21, 158–175.

Bonini, M., Souriot, T., Boccaletti, M., Brun, J.P., 1997. Successive orthogonal and oblique extension episodes in a rift zone: laboratory experiments with application to the Ethiopian Rift. Tectonics 16, 347–362.

Bonini, M., Sokoutis, D., Mulugeta, G., Katrivanos, E., 2000. Modelling hanging wall accommodation above rigid thrust ramps. J. Struct. Geol. 22, 1165–1179.

Bonini, M., Sokoutis, D., Mulugeta, G., Boccaletti, M., Corti, G., Innocenti, F., Manetti, P., Mazzarini, F., 2001. Dynamics of magma emplacement in centrifuge models of continental extension with implications for flank volcanism. Tectonics 20, 1053–1065.

Bonini, M., Corti, G., Sokoutis, D., Vannucci, G., Gasperini, P., Cloetingh, S., 2003. Insights from scaled analogue modelling into the seismotectonics of the Iranian region. Tectonophysics 376, 137–149.

Bonini, M., 2007. Deformation patterns and structural vergence in brittle-ductile thrust wedges: an additional analogue modelling perspective. J. Struct. Geol. 29, 141–158, http://dx.doi.org/10.1016/j.jsg.2006.06.012.

Bonnet, C., Malavieille, J., Mosar, J., 2007. Interactions between tectonics, erosion, and sedimentation during the recent evolution of the Alpine orogen: analogue modeling insights. Tectonics 26, TC6016, http://dx.doi.org/10.1029/2006tc002048.

Bose, S., Saha, P., Mori, J.J., Rowe, C., Ujiie, K., Chester, F.M., Conin, M., Regalla, C., Kameda, J., Toy, V., Kirkpatrick, J., Remitti, F., Moore, J.C., Wolfson-Schwehr, M., Nakamura, Y., Gupta, A., 2015. Deformation structures in the frontal prism near the Japan Trench:Insights from sandbox models. J. Geodyn. 89, 29–38.

Boutelier, D.A., Chemenda, A.I., 2008. Exhumation of UHP/LT rocks due to the local reduction of the interplate pressure: thermo-mechanical physical modelling. Earth Planet. Sci. Lett. 271, 226–232.

Boutelier, D.A., Cruden, A.R., 2008. Impact of regional mantle flow on subducting plate geometry and interplate stress: insights from physical modelling. Geophys. J. Int. 174, 719–732.

Boutelier, D., Cruden, A., 2013. Slab rollback rate and trench curvature controlled by arc deformation. Geology 41, 911–914, http://dx.doi.org/10.1130/G34338.1.

Boutelier, D., Oncken, O., 2011. 3-D thermo-mechanical laboratory modeling of plate-tectonics: modeling scheme, technique and first experiments. Solid Earth 2, 35–51.

Boutelier, D., Chemenda, A., Burg, J.-P., 2003. Subduction versus accretion of intra-oceanic volcanic arcs: insight from thermo-mechanical analogue experiments. Earth Planet. Sci. Lett. 212, 31–45, http://dx.doi.org/10.1016/S0012-821X(03)00239-5.

Boutelier, D., Schrank, C., Cruden, A., 2008. Power-law viscous materials for analogue experiments: new data on the rheology of highly-filled silicone polymers. J. Struct. Geol. 30, 341–353.

Brace, W.F., Byerlee, J.D., 1966. Stick-slip as a mechanism for earthquakes. Science 153, 990–992.

Brun, J.-P., Fort, X., 2011. Salt tectonics at passive margins: geology versus models. Mar. Petrol. Geol. 28, 1123–1145, http://dx.doi.org/10.1016/j.marpetgeo.2011.03.004.

Brun, J.-P., 1999. Narrow rifts versus wide rifts: Inferences for the mechanics of rifting from laboratory experiments. Philos. Trans. R. Soc. A: Math. Phys. Eng. Sci. 357, 695–712.

Brun, J.P., Sokoutis, D., Van Den Driessche, J., 1994. Analogue modeling of detachment fault systems and core complexes. Geology 22, 319–322.

Brune, J.N., Ellis, M.A., 1997. Structural features in a brittle-ductile wax model of continental extension. Nature 387, 67–70.

Buck, W.R., Sokoutis, D., 1994. Analogue model of gravitational collapse and surface extension during continental convergence. Nature 369, 737–740.

Burg, J.-P., Sokoutis, D., Bonini, M., 2002. Model-inspired interpretation of seismic structures in the Central Alps: crustal wedging and buckling at mature stage of collision. Geology 30, 643–646.

Burliga, S., Koyi, H.A., Chemia, Z., 2012. Analogue and numerical modelling of salt supply to a diapiric structure rising above an active basement fault. Geol. Soc. Lond. Special Publ. 363, 395–408.

Busse, F.H., Whitehead, J.A., 1971. Instabilities of convection rolls in a high Prandtl number fluid. J. Fluid Mech. 47, 305–320.

Buttles, J., Olson, P., 1998. A laboratory model of subduction zone anisotropy. Earth Planet. Sci. Lett. 164, 245–262.

Byerlee, J., 1978. Friction of rocks. Pure Appl. Geophys. 116, 615–626.

Cadell, H.M., 1889. Experimental researches in mountain building. Tans. R. Soc. Edinburgh 1, 339–343.

Cagnard, F., Durrieu, N., Gapais, D., Brun, J.P., Ehlers, C., 2006. Crustal thickening and lateral flow during compression of hot lithospheres, with particular reference to Precambrian times. Terra Nova 18, 72–78.

Calignano, E., Sokoutis, D., Willingshofer, E., Gueydan, F., Cloetingh, S., 2015. Asymmetric vs: symmetric deep lithospheric architecture of intra-plate continental orogens. Earth Planet. Sci. Lett. 424, 38–50, http://dx.doi.org/10.1016/j.epsl.2015.05.022.

Caniven, Y., Dominguez, S., Soliva, R., Cattin, R., Peyret, M., Marchandon, M., Romano, C., Strak, V., 2015. A new multilayered visco-elasto-plastic experimental model to study strike-slip fault seismic cycle. Tectonics 34, 232–264.

Cardozo, N., Allmendinger, R.W., 2009. SSPX: A program to compute strain from displacement/velocity data. Comp. Geosci. 35, 1343–1357.

Carter, N.L., 1976. Steady state flow of rocks. Rev. Geophys. Space Phys. 14, 301–360.

Casas, A.M., Gapais, D., Nalpas, T., Besnard, K., Román-Berdiel, T., 2001. Analogue models of transpressive systems. J. Struct. Geol. 23, 733–743.

Cerca, M., Manetti, P., Ferrari, L., Bonini, M., Corti, G., 2004. The role of crustal heterogeneity in controlling vertical coupling during Laramide shortening and the development of the Caribbean–North America transform boundary in southern Mexico: insights from analogue models. Geol. Soc. Lond. 227, 117–140 (Special Publications).

Chemenda, A.I., Mattauer, M., Malavieille, J., Bokun, A.N., 1995. A mechanism for syn-collisional rock exhumation and associated normal faulting: results from physical modelling. Earth Planet. Sci. Lett. 132, 225–232.

Chemenda, A.I., Mattauer, M., Bokun, A.N., 1996. Continental subduction and a mechanism for exhumation of high-pressure metamorphic rocks: new modelling and field data from Oman. Earth Planet. Sci. Lett. 143, 173–182.

Chemenda, A.I., Burg, J.P., Mattauer, M., 2000. Evolutionary model of the Himalaya-Tibet system: geopoem based on new modelling. Geol. Geophys. Data.

Chen, Z., Schellart, W.P., Duarte, J.C., 2015a. Quantifying the energy dissipation of overriding plate deformation in three-dimensional subduction models. J. Geophys. Res. Solid Earth 120, 519–536, http://dx.doi.org/10.1002/2014JB011419.

Chen, Z., Schellart, W.P., Duarte, J.C., 2015b. Overriding plate deformation and variability of fore-arc deformation during subduction: insight from geodynamic models and application to the Calabria subduction zone. Geochem. Geophys. Geosyst. 16, 3697–3715, http://dx.doi.org/10.1002/2015GC005958.

Chen, Z., Schellart, W.P., Strak, V., Duarte, J.C., 2016. Does subduction-induced mantle flow drive backarc extension? Earth Planet. Sci. Lett., http://dx.doi.org/10.1016/j.epsl.2016.02.027.

Cloos, E., 1955. Experimental analysis of fracture patterns. Geol. Soc. Am. Bull. 66, 241–256.

Cobbold, P.R., Castro, L., 1999. Fluid pressure and effective stress in sandbox models. Tectonophysics 301, 1–19.

Cobbold, P.R., Jackson, M.P.A., 1992. Gum rosin (colophony): a suitable material for thermomechanical modelling of the lithosphere. Tectonophysics 210, 255–271.

Cobbold, P.R., 1975. Fold propagation in single embedded layers. Tectonophysics 27, 333–351.

Colletta, B., Letouzey, J., Pinedo, R., Ballard, J.F., Balé, P., 1991. Computerized X-ray tomography analysis of sandbox models: examples of thin-skinned thrust systems. Geology 19, 1063–1067.

Corbi, F., Funiciello, F., Moroni, M., Dinther, Y., Mai, P.M., Dalguer, L.A., Faccenna, C., 2013. The seismic cycle at subduction thrusts: 1. Insights from laboratory models. J. Geophys. Res. Solid Earth 118, 1483–1501.

Corti, G., Manetti, P., 2006. Asymmetric rifts due to asymmetric Mohos: an experimental approach. Earth Planet. Sci. Lett. 245, 315–329.

Corti, G., Bonini, M., Conticelli, S., Innocenti, F., Manetti, P., Sokoutis, D., 2003. Analogue modelling of continental extension: a review focused on the relations between the patterns of deformation and the presence of magma. Earth Sci. Rev. 63, 169–247, http://dx.doi.org/10.1016/S0012-8252(03)00035-7.

Corti, G., Ranalli, G., Mulugeta, G., Agostini, A., Sani, F., Zugu, A., 2010. Control of the rheological structure of the lithosphere on the inward migration of tectonic activity during continental rifting. Tectonophysics 490, 165–172, http://dx.doi.org/10.1016/j.tecto.2010.05.004.

Corti, G., 2008. Control of rift obliquity on the evolution and segmentation of the main Ethiopian rift. Nat. Geosci. 1, 258–262, http://dx.doi.org/10.1038/ngeo160.

Cotton, J.T., Koyi, H.A., 2000. Modeling of thrust fronts above ductile and frictional detachments: application to structures in the Salt Range and Potwar Plateau, Pakistan. Geol. Soc. Am. Bull. 112, 351–363.
Coulomb, C.A., 1773. Essai sur une application des règles de maximis et minimis à quelques problèmes de statique relatifs à l'architecture. Mémoires de Mathématiques et de Physique Académie Royale des Sciences 7, 343–382.
Cruden, A.R., Nasseri, M.H.B., Pysklywec, R., 2006. Surface topography and internal strain variation in wide hot orogens from three-dimensional analogue and two-dimensional numerical vice models. Geol. Soc. Lond. Special Publ. 253, 79–104.
Cruz, L., Teyssier, C., Perg, L., Take, A., Fayon, A., 2008. Deformation, exhumation, and topography of experimental doubly-vergent orogenic wedges subjected to asymmetric erosion. J. Struct. Geol. 30, 98–115.
Darbouli, M., Métivier, C., Piau, J.M., Magnin, A., Abdelali, A., 2013. Rayleigh-Bénard convection for viscoplastic fluids. Phys. Fluids 25, 023101.
Daubre, A., 1879. Etudes synthétiques de géologie expérimentale, pt 1., Dunod Paris.
Davaille, A., Jaupart, C., 1993. Transient high-Rayleigh-number thermal convection with large viscosity variations. J. Fluid Mech. 253, 141–166.
Davaille, A., Limare, A., 2007. Laboratory studies of mantle convection. Treatise. Geophys. 7, 89–165.
Davaille, A., Vatteville, J., 2005. On the transient nature of mantle plumes. Geophys. Res. Lett. 32, http://dx.doi.org/10.1029/2005gl023029.
Davaille, A., Girard, F., Le Bars, M., 2002. How to anchor hotspots in a convecting mantle? Earth Planet. Sci. Lett. 203, 621–634.
Davaille, A., Limare, A., Touitou, F., Kumagai, I., Vatteville, J., 2011. Anatomy of a laminar starting thermal plume at high Prandtl number. Exp. Fluids 50, 285–300.
Davaille, A., Gueslin, B., Massmeyer, A., Di Giuseppe, E., 2013. Thermal instabilities in a yield stress fluid: existence and Morphology. J. Non-Newtonian Fluid Mech. 193, 144–153.
Davy, P., Cobbold, P.R., 1988. Indentation tectonics in nature and experiment 1. Experiments scaled for gravity. Bull. Geol. Inst. Univ. Uppsala 14, 129–141.
Davy, P., Cobbold, P.R., 1991. Experiments on shortening of a 4-layer model of the continental lithosphere. Tectonophysics 188, 1–25.
Dell'Ertole, D., Schellart, W.P., 2013. The development of sheath folds in viscously stratified materials in simple shear conditions: an analogue approach. J. Struct. Geol. 56, 129–141, http://dx.doi.org/10.1016/j.jsg.2013.09.002.
Di Giuseppe, E., Funiciello, F., Corbi, F., Ranalli, G., Mojoli, G., 2009. Gelatins as rock analogs: a systematic study of their rheological and physical properties. Tectonophysics 473, 391–403.
Di Giuseppe, E., Corbi, F., Funiciello, F., Massmeyer, A., Santimano, T.N., Rosenau, M., Davaille, A., 2015. Characterization of Carbopol® hydrogel rheology for experimental tectonics and geodynamics. Tectonophysics 642, 29–45.
Dietl, C., Koyi, H., 2011. Sheets within diapirs—results of a centrifuge experiment. J. Struct. Geol. 33, 32–37, http://dx.doi.org/10.1016/j.jsg.2010.10.010.
Dixon, J.M., Summers, J.M., 1985. Recent developments in centrifuge modelling of tectonic processes: equipment, model construction techniques and rheology of model materials. J. Struct. Geol. 7, 83–102.
Dombrádi, E., Sokoutis, D., Bada, G., Cloetingh, S., Horváth, F., 2010. Modelling recent deformation of the Pannonian lithosphere: lithospheric folding and tectonic topography. Tectonophysics 484, 103–118, http://dx.doi.org/10.1016/j.tecto.2009.09.014.
Dominguez, S., Lallemand, S.E., Malavieille, J., von Huene, R., 1998. Upper plate deformation associated with seamount subduction. Tectonophysics 293, 207–224.
Donnadieu, F., Merle, O., 1998. Experiments on the indentation process during cryptodome intrusions: new insights into Mount St. Helens deformation. Geology 26, 79–82.
Donnadieu, F., Kelfoun, K., van Wyk de Vries, B., Cecci, E., Merle, O., 2003. Digital photogrammetry as a tool in analogue modelling: applications to volcano instability. J. Volcanol. Geotherm. Res. 123, 161–180.
Dooley, T.P., Schreurs, G., 2012. Analogue modelling of intraplate strike-slip tectonics: a review and new experimental results. Tectonophysics 574-575, 1–71, http://dx.doi.org/10.1016/j.tecto.2012.05.030.
Dooley, T.P., Jackson, M.P.A., Hudec, M.R., 2009. Inflation and deflation of deeply buried salt stocks during lateral shortening. J. Struct. Geol. 31, 582–600, http://dx.doi.org/10.1016/j.jsg.2009.03.013.
Druken, K.A., Long, M.D., Kincaid, C., 2011. Patterns in seismic anisotropy driven by rollback subduction beneath the High Lava Plains. Geophys. Res. Lett. 38, L13310, http://dx.doi.org/10.1029/2011gl047541.
Druken, K.A., Kincaid, C., Griffiths, R.W., Stegman, D.R., Hart, S.R., 2014. Plume–slab interaction: the Samoa–Tonga system. Phys. Earth Planet. Interiors 232, 1–14.
Duarte, J.C., Rosas, F.M., Terrinha, P., Gutscher, M.-A., Malavieille, J., Silva, S., Matias, L., 2011. Thrust–wrench interference tectonics in the Gulf of Cadiz (Africa–Iberia plate boundary in the North-East Atlantic): Insights from analog models. Mar. Geol. 289, 135–149, http://dx.doi.org/10.1016/j.margeo.2011.09.014.
Duarte, J.C., Schellart, W.P., Cruden, A.R., 2013. Three-dimensional dynamic laboratory models of subduction with an overriding plate and variable interplate rheology. Geophys. J. Int. 195, 47–66, http://dx.doi.org/10.1093/gji/ggt257.
Duarte, J.C., Schellart, W.P., Cruden, A.R., 2014. Rheology of petrolatum-paraffin oil mixtures: applications to analogue modelling of geological processes. J. Struct. Geol. 63, 1–11, http://dx.doi.org/10.1016/j.jsg.2014.02.004.
Dufréchou, G., Odonne, F., Viola, G., 2011. Analogue models of second-order faults genetically linked to a circular strike-slip system. J. Struct. Geol. 33, 1193–1205, http://dx.doi.org/10.1016/j.jsg.2011.04.002.
Edwards, S.J., Schellart, W.P., Duarte, J.C., 2015. Geodynamic models of continental subduction and obduction of overriding plate forearc oceanic lithosphere on top of continental crust. Tectonics 34, 1494–1515, http://dx.doi.org/10.1002/2015TC003884.
Eisenstadt, G., Sims, D., 2005. Evaluating sand and clay models: do rheological differences matter? J. Struct. Geol. 27, 1399–1412.
England, P., McKenzie, D., 1982. A thin viscous sheet model for continental deformation. Geophys. J. Int. 70, 295–321.
Escher, B.G., Kuenen, P.H., 1929. Experiments in connection with salt domes. Leidsche Geologische Mededeelingen 3, 151–182.
Faccenna, C., Davy, P., Brun, J.-P., Funiciello, R., Giardini, D., Mattei, M., Nalpas, T., 1996. The dynamics of back-arc extension; an experimental approach to the opening of the Tyrrhenian Sea. Geophys. J. Int. 126, 781–795.
Faccenna, C., Giardini, D., Davy, P., Argentieri, A., 1999. Initiation of subduction at Atlantic-type margins; insights from laboratory experiments. J. Geophys. Res. 104, 2749–2766.
Farzipour-Saein, A., Nilfouroushan, F., Koyi, H., 2013. The effect of basement step/topography on the geometry of the Zagros fold and thrust belt (SW Iran): an analog modeling approach. Int. J. Earth Sci. 102, 2117–2135.
Faugere, E.T., Brun, J.P., 1984. Modélisation expérimentale de la distention continentale Comptes-rendus des séances de l'Académie des sciences Série 2, Mécanique-physique, chimie. sciences de l'univers, sciences de la terre 299, 365–370.
Favre, A., 1878a. Expériences sur les effets des refoulements ou écrasements latéraux en géologie Comptes Rendus Hebdomadaires des Séances de l. 'Académie des Sciences T86, 1092–1095.
Favre, A., 1878b. Expériences sur les effets des refoulements ou écrasements latéraux en géologie La Nature. Archives des sciences physiques et naturelles 246, 278–283.
Fernández-Lozano, J., Sokoutis, D., Willingshofer, E., Cloetingh, S.A.P.L., De Vicente, G., 2011. Cenozoic deformation of Iberia: a model for intraplate mountain building and basin development based on analogue modeling. Tectonics 30, TC1001, http://dx.doi.org/10.1029/2010tc002719.
Ferrer, O., Roca, E., Vendeville, B.C., 2014. The role of salt layers in the hangingwall deformation of kinked-planar extensional faults: insights from 3D analogue models and comparison with the Parentis Basin. Tectonophysics 636, 338–350.
Fischer, M.P., Keating, D.P., 2005. Photogrammetric techniques for analyzing displacement, strain, and structural geometry in physical models: application to the growth of monoclinal basement uplifts. Geol. Soc. Am. Bull. 117, 369–382.
Fitzgerald, P.G., Muñoz, J.A., Coney, P.J., Baldwin, S.L., 1999. Asymmetric exhumation across the Pyrenean orogen: implications for the tectonic evolution of a collisional orogen. Earth Planet. Sci. Lett. 173, 157–170.
Forsyth, D.W., Uyeda, S., 1975. On the relative importance of the driving forces of plate motion. Geophys. J. R. Astron. Soc. 43, 163–200.
Fournier, M., Jolivet, L., Davy, P., Thomas, J.-C., 2004. Backarc extension and collision: an experimental approach to the tectonics of Asia. Geophys. J. Int. 157, 871–889, http://dx.doi.org/10.1111/j.1365-246X.2004.02223.x.
Funiciello, F., Faccenna, C., Giardini, D., Regenauer-Lieb, K., 2003. Dynamics of retreating slabs (part 2): Insights from 3-D laboratory experiments. J. Geophys. Res. 108 (B4) 2207, 2210, http://dx.doi.org/10.1029/2001JB000896.
Funiciello, F., Moroni, M., Piromallo, C., Faccenna, C., Cenedese, A., Bui, H.A., 2006. Mapping mantle flow during retreating subduction: laboratory models analyzed by feature tracking. J. Geophys. Res. 111, B03402, http://dx.doi.org/10.1029/2005jb003792.
Funiciello, F., Faccenna, C., Heuret, A., Lallemand, S., Di Giuseppe, E., Becker, T.W., 2008. Trench migration, net rotation and slab-mantle coupling. Earth Planet. Sci. Lett. 271, 233–240, http://dx.doi.org/10.1016/j.epsl.2008.04.006.
Göğüş, O.H., Pysklywec, R.N., Corbi, F., Faccenna, C., 2011. The surface tectonics of mantle lithosphere delamination following ocean lithosphere subduction: insights from physical-scaled analogue experiments. Geochem. Geophys. Geosyst. 12, Q05004, http://dx.doi.org/10.1029/2010GC003430.
Galland, O., de Bremond d'Ars, J., Cobbold, P.R., Hallot, E., 2003. Physical models of magmatic intrusion during thrusting. Terra Nova 15, 405–409, http://dx.doi.org/10.1046/j. 1365–3121.2003.00512.x.
Galland, O., Cobbold, P.R., Hallot, E., de Bremond d'Ars, J., Delavaud, G., 2006. Use of vegetable oil and silica powder for scale modelling of magmatic intrusion in a deforming brittle crust. Earth Planet. Sci. Lett. 243, 786–804.
Galland, O., Planke, S., Neumann, E.-R., Malthe-Sørenssen, A., 2009. Experimental modelling of shallow magma emplacement: application to saucer-shaped intrusions. Earth Planet. Sci. Lett. 277, 373–383, http://dx.doi.org/10.1016/j.epsl.2008.11.003.
Gartrell, A.P., 1997. Evolution of rift basins and low-angle detachments in multilayer analog models. Geology 25, 615–618.
Gautier, P., Brun, J.-P., Moriceau, R., Sokoutis, D., Martinod, J., Jolivet, L., 1999. Timing, kinematics and cause of Aegean extension; a scenario based on a comparison with simple analogue experiments. Tectonophysics 315, 31–72.
Gibson, J.J., 1950. The Perception of the Visual World. Riverside Press, Cambridge.
Godin, L., Yakymchuk, C., Harris, L.B., 2011. Himalayan hinterland-verging superstructure folds related to foreland-directed infrastructure ductile flow: insights from centrifuge analogue modelling. J. Struct. Geol. 33, 329–342.
Gomes, C.J.S., 2013. Investigating new materials in the context of analog-physical models. J. Struct. Geol. 46, 158–166.

Goren, L., Aharonov, E., Mulugeta, G., Koyi, H.A., Mart, Y., 2008. Ductile deformation of passive margins: a new mechanism for subduction initiation. J. Geophys. Res. 113, B08411, http://dx.doi.org/10.1029/2005jb004179.
Grant, I., 1997. Particle image velocimetry: a review. Proc. Inst. Mech. Eng. Part C: J. Mech. Eng. Sci. 211, 55–76.
Graveleau, F., Dominguez, S., 2008. Analogue modelling of the interaction between tectonics, erosion and sedimentation in foreland thrust belts. C.R. Geosci. 340, 324–333.
Graveleau, F., Dominguez, S., Malavieille, J., 2008. A new analogue modelling approach for studying interactions between surface processes and deformation in active mountain belt piedmonts. Bollettino di Geofisica Teorica ed Applicata 49 (suppl. 2), 501–505.
Graveleau, F., Hurtrez, J.E., Dominguez, S., Malavieille, J., 2011. A new experimental material for modeling relief dynamics and interactions between tectonics and surface processes. Tectonophysics 513, 68–87.
Graveleau, F., Malavieille, J., Dominguez, S., 2012. Experimental modelling of orogenic wedges: a review. Tectonophysics 538-540, 1–66, http://dx.doi.org/10.1016/j.tecto.2012.01.027.
Graveleau, F., Strak, V., Dominguez, S., Malavieille, J., Chatton, M., Manighetti, I., Petit, C., 2015. Experimental modelling of tectonics–erosion–sedimentation interactions in compressional, extensional, and strike–slip settings. Geomorphology 244, 146–168, http://dx.doi.org/10.1016/j.geomorph.2015.02.011.
Griffiths, R.W., Campbell, I.H., 1990. Stirring and structure in mantle starting plumes. Earth Planet. Sci. Lett. 99, 66–78.
Griffiths, R.W., Hackney, R.I., van der Hilst, R.D., 1995. A laboratory investigation of effects of trench migration on the descent of subducted slabs. Earth Planet. Sci. Lett. 133, 1–17.
Griffiths, R.W., 1986. Thermals in extremely viscous fluids, incuding the effects of temperature-dependent viscosity. J. Fluid Mech. 166, 115–138.
Griggs, D., 1939. A theory of mountain-building. Am. J. Sci. 237, 611–650.
Grujic, D., Mancktelow, N.S., 1998. Melt-bearing shear zones: analogue experiments and comparison with examples from southern Madagascar. J. Struct. Geol. 20, 673–680.
Guillaume, B., Martinod, J., Espurt, N., 2009. Variations of slab dip and overriding plate tectonics during subduction: insights from analogue modelling. Tectonophysics 463, 167–174, http://dx.doi.org/10.1016/j.tecto.2008.09.043.
Guillaume, B., Funiciello, F., Faccenna, C., Martinod, J., Olivetti, V., 2010. Spreading pulses of the Tyrrhenian Sea during the narrowing of the Calabrian slab. Geology 38, 819–822, http://dx.doi.org/10.1130/G31038.1.
Guillou-Frottier, L., Buttles, J., Olson, P., 1995. Laboratory experiments on the structure of subducted lithosphere. Earth Planet. Sci. Lett. 133, 19–34.
Gutscher, M.-A., Kukowski, N., Malavieille, J., Lallemand, S., 1998. Episodic imbricate thrusting and underthrusting: analog experiments and mechanical analysis applied to the Alaskan accretionary wedge. J. Geophys. Res. 103, 10161–10176.
Hall, J., 1815. On the vertical position and convolutions of certain strata and their relationship with granite. Trans. R. Soc. Edinburgh 7, 79–108.
Hampel, A., Adam, J., Kukowski, N., 2004. Response of the tectonically erosive south Peruvian forearc to subduction of the Nazca Ridge: analysis of three-dimensional analogue experiments. Tectonics 23, TC5003, http://dx.doi.org/10.1029/2003tc001585.
Harris, L.B., Koyi, H.A., 2002. Centrifuge modelling of folding in high-grade rocks during rifting. J. Struct. Geol. 25, 291–305.
Hatzfeld, D., Martinod, J., Bastet, G., Gautier, P., 1997. An analog experiment for the Aegean to describe the contribution of gravitational potential energy. J. Geophys. Res. 102, 649–659.
Heuret, A., Funiciello, F., Faccenna, C., Lallemand, S., 2007. Plate kinematics, slab shape and back-arc stress: a comparison between laboratory models and current subduction zones. Earth Planet. Sci. Lett. 256, 473–483.
Hirth, G., Tullis, J., 1992. Dislocation creep regimes in quartz aggregates. J. Struct. Geol. 14, 145–159.
Horn, B.K., Schunck, B.G., 1981. Determining optical flow Technical symposium east. Int. Soc. Opt. Photon., 319–331.
Horsfield, W., 1977. An experimental approach to basement-controlled faulting. Geol. Mijnbouw 56, 363–370.
Hoth, S., Adam, J., Kukowski, N., Oncken, O., 2006. Influence of erosion on the kinematics of bivergent orgens. Results from scaled sandbox simulations. In: Willett, S.D., Hovius, N., Brandon, M.T., Fisher, D.M. (Eds.), Tectonics, Climate, and Landscape Evolution. Geological Society of America Boulder, pp. 201–225.
Hoth, S., Hoffmann-Rothe, A., Kukowski, N., 2007. Frontal accretion: an internal clock for bivergent wedge deformation and surface uplift. J. Geophys. Res. 112, http://dx.doi.org/10.1029/2006jb004357 (B06408).
Hoth, S., Kukowski, N., Oncken, O., 2008. Distant effects in bivergent orogenic belts – how retro-wedge erosion triggers resource formation in pro-foreland basins. Earth Planet. Sci. Lett. 273, 28–37.
Hubbert, M.K., 1937. Theory of scale models as applied to the study of geologic structures. Geol. Soc. Am. Bull. 48, 1459–1520.
Hubbert, M.K., 1951. Mechanical basis for certain familiar geologic structures. Geol. Soc. Am. Bull. 62, 355–372.
Hudson, J.D., Dennis, S.C.R., 1985. The flow of a viscous incompressible fluid past a normal flat plate at low and intermediate Reynolds numbers: the wake. J. Fluid Mech. 160, 369–383.
Husson, L., Guillaume, B., Funiciello, F., Faccenna, C., Royden, L.H., 2012. Unraveling topography around subduction zones from laboratory models. Tectonophysics 526, 5–15.
Ildefonse, B., Sokoutis, D., Mancktelow, N.S., 1992. Mechanical interactions between rigid particles in a deforming ductile matrix. Analogue experiments in simple shear flow. J. Struct. Geol. 14, 1253–1266.
Irvine, D.N., Schellart, W.P., 2012. Effect of plate thickness on bending radius and energy dissipation at the subduction zone hinge. J. Geophys. Res. 117, http://dx.doi.org/10.1029/2011jb009113 (B06405).
Jacoby, W.R., 1973. Model experiment of plate movements. Nature Phys. Sci. 242, 130–134.
Jacoby, W.R., 1976. Paraffin model experiment of plate tectonics. Tectonophysics 35, 103–113.
Jellinek, A.M., Gonnermann, H.M., Richards, M.A., 2003. Plume capture by divergent plate motions: implications for the distribution of hotspots, geochemistry of mid-ocean ridge basalts, and estimates of the heat flux at the core-mantle boundary. Earth Planet. Sci. Lett. 205, 361–378.
Kavanagh, J.L., Boutelier, D., Cruden, A.R., 2015. The mechanics of sill inception, propagation and growth: experimental evidence for rapid reduction in magmatic overpressure. Earth Planet. Sci. Lett. 421, 117–128.
Kebiche, Z., Castelain, C., Burghelea, T., 2014. Experimental investigation of the Rayleigh–Bénard convection in a yield stress fluid. J. Non-Newtonian Fluid Mech. 203, 9–23.
Keep, M., McClay, K.R., 1997. Analogue modelling of multiphase rift systems. Tectonophysics 273, 239–270.
Keep, M., 2000. Models of lithospheric-scale deformation during plate collision: effects of indentor shape and lithospheric thickness. Tectonophysics 326, 203–216.
Keep, M., 2003. Physical modelling of deformation in the Tasman Orogenic Zone. Tectonophysics 375, 37–47, http://dx.doi.org/10.1016/j.tecto.2003.06.002.
Kerr, R.C., Mériaux, C., 2004. Structure and dynamics of sheared mantle plumes. Geochemistry Geophysics Geosystems 5, Q12009, http://dx.doi.org/10.1029/2004gc000749.
Kervyn, M., Ernst, G.G.J., van Wyk de Vries, B., Mathieu, L., Jacobs, P., 2009. Volcano load control on dyke propagation and vent distribution: insights from analogue modeling. J. Geophys. Res. 114, B03401, http://dx.doi.org/10.1029/2008jb005653.
Kincaid, C., Griffiths, R.W., 2003. Laboratory models of the thermal evolution of the mantle during rollback subduction. Nature 425, 58–62.
Kincaid, C., Griffiths, R.W., 2004. Variability in flow and temperatures within mantle subduction zones. Geochem. Geophys. Geosyst. 5, Q06002, http://dx.doi.org/10.1029/2003gc000666.
Kincaid, C., Olson, P., 1987. An experimental study of subduction and slab migration. J. Geophys. Res. 92 (13), 13832–13840.
Kirby, S.H., Kronenberg, A.K., 1987. Rheology of the lithosphere: selected topics. Rev. Geophys. 25, 1219–1244.
Kirby, S.H., 1985. Rock mechanics observations pertinent to the rheology of the continental lithosphere and the localisation of strain along shear zones. Tectonophysics 119, 1–27.
Kobberger, G., Zulauf, G., 1995. Experimental folding and boudinage under pure constrictional conditions. J. Struct. Geol. 17, 1055–1063.
Kohlstedt, D.L., Evans, B., Mackwell, S.J., 1995. Strength of the lithosphere: constraints imposed by laboratory experiments. J. Geophys. Res. 100, 17–587.
Konstantinovskaia, E., Malavieille, J., 2005. Erosion and exhumation in accretionary orogens: experimental and geological approaches. Geochem. Geophys. Geosyst. 6, http://dx.doi.org/10.1029/2004gc000794 (Q02006).
Konstantinovskaya, E.A., Rodriguez, D., Kirkwood, D., Harris, L.B., Thériault, R., 2009. Effects of basement structure, sedimentation and erosion on thrust wedge geometry: an example from the Quebec Appalachians and analogue models. Bull. Can. Petrol. Geol. 57, 34–62.
Koyi, H.A., Vendeville, B.C., 2003. The effect of décollement dip on geometry and kinematics of model accretionay wedges. J. Struct. Geol. 25, 1445–1450.
Koyi, H.A., Ghasemi, A., Hessami, K., Dietl, C., 2008. The mechanical relationship between strike-slip faults and salt diapirs in the Zagros fold–thrust belt. J. Geol. Soc. Lond. 165, 1031–1044.
Koyi, H., 1995. Mode of internal deformation in sand wedges. J. Struct. Geol. 17, 293–300.
Koyi, H., 1997. Analogue modelling; from a qualitative to a quantitative technique; a historical outline. J. Pet. Geol 20, 223–238.
Koyi, H.A., 2001. Modeling the influence of sinking anhydrite blocks on salt diapirs targeted for hazardous waste disposal. Geology 29, 387–390.
Krantz, R.W., 1991. Measurements of friction coefficients and cohesion for faulting and fault reactivation in laboratory models using sand and sand mixtures. Tectonophysics 188, 203–207.
Krawczyk, C.M., Buddensiek, M.L., Oncken, O., Kukowski, N., 2013. Seismic imaging of sandbox experiments—laboratory hardware setup and first reflection seismic sections. Solid Earth 4, 93–104.
Kuenen, P.H., de Sitter, L.U., 1938. Experimental investigation into the mechanism of folding. Leidse Geologische Mededelingen 10, 217–239.
Kuenen, P.H., 1936. The negative isostatic anomalies in the East Indies (with experiments). Leidse Geologische Mededeelingen 8, 169–214.
Kukowski, N., Lallemand, S.E., Malavieille, J., Gutscher, M.-A., Reston, T.J., 2002. Mechanical decoupling and basal duplex formation observed in sandbox experiments with application to the Western Mediterranean Ridge accretionary complex. Mar. Geol. 186, 29–42.
Kumagai, I., Davaille, A., Kurita, K., 2007. On the fate of thermally buoyant mantle plumes at density interfaces. Earth Planet. Sci. Lett. 254, 180–193, http://dx.doi.org/10.1016/j.epsl.2006.11.029.

Lagabrielle, Y., Garel, E., Dauteuil, O., Cormier, M.H., 2001. Extensional faulting and caldera collapse in the axial region of fast spreading ridges: analog modeling. J. Geophys. Res. 106, 2005–2015.
Lallemand, S.E., Malavieille, J., Calassou, S., 1992. Effects of oceanic ridge subduction on accretionary wedges: experimental modeling and marine observations. Tectonics 11, 1301–1313.
Lama, R.D., Vutukuri, V.S., 1978. Handbook on Mechanical Properties of Rocks Testing Techniques and Results. Clausthal, Germany.
Le Bars, M., Davaille, A., 2004. Whole layer convection in a heterogeneous planetary mantle. J. Geophys. Res. 109, B03403, http://dx.doi.org/10.1029/2003jb002617.
Le Guerroué, E., Cobbold, P.R., 2006. Influence of erosion and sedimentation on strike-slip fault systems: insights from analogue models. J. Struct. Geol. 28, 421–430, http://dx.doi.org/10.1016/j.jsg.2005.11.007.
Leever, K.A., Gabrielsen, R.H., Sokoutis, D., Willingshofer, E., 2011. The effect of convergence angle on the kinematic evolution of strain partitioning in transpressional brittle wedges: insight from analog modeling and high-resolution digital image analysis. Tectonics 30, TC2013, http://dx.doi.org/10.1029/2010TC002823.
Leturmy, P., Mugnier, J.L., Vinour, P., Baby, P., Colletta, B., Chabron, E., 2000. Piggyback basin development above a thin-skinned thrust belt with two detachment levels as a function of interactions between tectonic and superficial mass transfer: the case of the Subandean Zone (Bolivia). Tectonophysics 320, 45–67.
Li, Z.-H., Ribe, N.M., 2012. Dynamics of free subduction from 3-D boundary element modeling. J. Geophys. Res. 117, B06408, http://dx.doi.org/10.1029/2012jb009165.
Link, T.A., 1930. Experiments relating to salt-dome structures. Bull. Am. Assoc. Petrol. Geol. 14, 483–508.
Lohrmann, J., Kukowski, N., Adam, J., Oncken, O., 2003. The impact of analogue material properties on the geometry, kinematics, and dynamics of convergent sand wedges. J. Struct. Geol. 25, 1691–1711.
Loiselet, C., Husson, L., Braun, J., 2009. From longitudinal slab curvature to slab rheology. Geology 37, 747–750, http://dx.doi.org/10.1130/G30052A.1.
Lu, C.Y., Malavieille, J., 1994. Oblique convergence, indentation and rotation tectonics in the Taiwan Mountain Belt: insights from experimental modelling. Earth Planet. Sci. Lett. 121, 477–494.
Luján, M., Storti, F., Rossetti, F., Crespo-Blanc, A., 2006. Extrusion vs: accretion at the frictional–viscous décollement transition in experimental thrust wedges: the role of convergence velocity. Terra Nova 18, 241–247, http://dx.doi.org/10.1111/j. 1365–3121.2006.00685.x.
Luth, S., Willingshofer, E., Sokoutis, D., Cloetingh, S., 2013a. Does subduction polarity changes below the Alps? Inferences from analogue modelling. Tectonophysics 582, 140–161, http://dx.doi.org/10.1016/j.tecto.2012.09.028.
Luth, S., Willingshofer, E., Ter Borgh, M., Sokoutis, D., Van Otterloo, J., Versteeg, A., 2013b. Kinematic analysis and analogue modelling of the Passeier and Jaufen faults: implications for crustal indentation in the Eastern Alps. Int. J. Earth Sci. 102, 1071–1090.
Lyell, C., 1871. The Student's Elements of Geology. John Murray, London.
Lyman, A.W., Kerr, R.C., Griffiths, R.W., 2005. Effects of internal rheology and surface cooling on the emplacement of lava flows. J. Geophys. Res. 110, B08207, http://dx.doi.org/10.1029/2005jb003643.
Mériaux, C.A., Duarte, J.C., Duarte, S.S., Schellart, W.P., Chen, Z., Rosas, F., Mata, J., Terrinha, P., 2015a. Capture of the Canary mantle plume material by the Gibraltar arc mantle wedge during slab rollback. Geophys. J. Int. 201, 1717–1721, http://dx.doi.org/10.1093/gji/ggv120.
Mériaux, C.A., Duarte, J.C., Schellart, W.P., Mériaux, A.-S., 2015b. A two-way interaction between the Hainan plume and the Manila subduction zone. Geophys. Res. Lett. 42, 5796–5802, http://dx.doi.org/10.1002/2015GL064313.
MacDougall, J.G., Kincaid, C., Szwaja, S., Fischer, K.M., 2014. The impact of slab dip variations, gaps and rollback on mantle wedge flow: insights from fluids experiments. Geophys. J. Int. 197, 705–730, http://dx.doi.org/10.1093/gji/ggu053.
Maerten, L., Maerten, F., 2006. Chronologic modeling of faulted and fractured reservoirs using geomechanically based restoration: technique and industry applications. AAPG Bull. 90, 1201–1226.
Malavieille, J., 1993. Late orogenic extension in mountain belts: insights from the Basin and Range and the late Paleozoic Variscan belt. Tectonics 12, 1115–1130.
Malavieille, J., 2010. Impact of erosion, sedimentation, and structural heritage on the structure and kinematics of orogenic wedges: analog models and case studies. GSA Today 20, 4–10.
Mancktelow, N.S., Arbaret, L., Pennacchioni, G., 2002. Experimental observations on the effect of interface slip on rotation and stabilisation of rigid particles in simple shear and a comparison with natural mylonites. J. Struct. Geol. 24, 567–585.
Mancktelow, N.S., 1988. The Rheology of paraffin wax and its usefulness as an analogue for rocks. Bull. Geol. Inst. Univ. Uppsala 14, 181–193.
Mandl, G., de Jong, L.N.J., Maltha, A., 1977. Shear zones in granular materials. Rock Mech. 9, 95–144.
Mandl, G., 1988. Mechanics of Tectonic Faulting: Models and Basic Concepts. Elsevier, Amsterdam.
Marques, F.O., Cobbold, P.R., 2002. Topography as a major factor in the development of arcuate thrust belts: insights from sandbox experiments. Tectonophysics 384, 247–268.
Marques, F.O., Cobbold, P.R., 2006. Effects of topography on the curvature of fold-and-thrust belts during shortening of a 2-layer model of continental lithosphere. Tectonophysics 415, 65–80.
Marques, F.O., Guerreiro, S.M., Fernandes, A.R., 2008. Sheath fold development with viscosity contrast: analogue experiments in bulk simple shear. J. Struct. Geol. 30, 1348–1353, http://dx.doi.org/10.1016/j.jsg.2008.07.001.
Marques, F.O., Fonseca, P.D., Lechmann, S., Burg, J.-P., Marques, A.S., Andrade, A.J.M., Alves, C., 2012. Boudinage in nature and experiment. Tectonophysics 526-529, 88–96, http://dx.doi.org/10.1016/j.tecto.2011.08.017.
Marques, F.O., 2008. Thrust initiation and propagation during shortening of a 2-layer model lithosphere. J. Struct. Geol. 30, 29–38, http://dx.doi.org/10.1016/j.jsg.2007.09.005.
Mart, Y., Aharonov, E., Mulugeta, G., Ryan, W., Tentler, T., Goren, L., 2005. Analogue modelling of the initiation of subduction. Geophys. J. Int. 160, 1081–1091.
Martinod, J., Davy, P., 1994. Periodic instabilities during compression of the lithosphere: 2. Analogue experiments. J. Geophys. Res. 99, 12057–12069.
Martinod, J., Hatzfeld, D., Brun, J.P., Davy, P., Gautier, P., 2000. Continental collision, gravity spreading, and kinematics of Aegea and Anatolia. Tectonics 19, 290–299.
Martinod, J., Guillaume, B., Espurt, N., Faccenna, C., Funiciello, F., Regard, V., 2013. Effect of aseismic ridge subduction on slab geometry and overriding plate deformation: insights from analogue modeling. Tectonophysics 588, 39–55, http://dx.doi.org/10.1016/j.tecto.2012.12.010.
Mathieu, L., van Wyk de Vries, B., Holohan, E.P., Troll, V.R., 2008. Dykes, cups, saucers and sills: analogue experiments on magma intrusion into brittle rocks. Earth Planet. Sci. Lett. 271, 1–13, http://dx.doi.org/10.1016/j.epsl.2008.02.020.
McClay, K., Dooley, T., 1995. Analogue models of pull-apart basins. Geology 23, 711–714.
McClay, K.R., Dooley, T., Lewis, G., 1998. Analog modeling of progradational delta systems. Geology 26, 771–774.
McClay, K.R., 1976. The rheology of plasticine. Tectonophysics 33, T7–15.
McClay, K.R., 1990. Extensional fault systems in sedimentary basins: a review of analogue model studies. Mar. Petrol. Geol. 7, 206–233.
Mead, W.J., 1920. Notes on the mechanics of geologic structures. J. Geol. 28, 505–523.
Merle, O., Abidi, N., 1995. Approche expérimentale du fonctionnement des rampes émergentes. Bull. Soc. Geol. Fr. 166, 439–450.
Merle, O., Guillier, B., 1989. The building of the Central Swiss Alps: an experimental approach. Tectonophysics 165, 41–56.
Merle, O., 1989. Strain models within spreading nappes. Tectonophysics 165, 57–71.
Meunier, S. 1904. La géologie expérimentale. Alcan Paris.
Meyer, C., Schellart, W.P., 2013. Three-dimensional dynamic models of subducting plate-overriding plate-upper mantle interaction. J. Geophys. Res. Solid Earth 118, 775–790, http://dx.doi.org/10.1002/jgrb.50078.
Michon, L., Sokoutis, D., 2005. Interaction between structural inheritance and extension direction during graben and depocentre formation: an experimental approach. Tectonophysics 409, 125–146.
Montanari, D., Corti, G., Sani, F., Del Ventisette, C., Bonini, M., Moratti, G., 2010. Experimental investigation on granite emplacement during shortening. Tectonophysics 484, 147–155, http://dx.doi.org/10.1016/j.tecto.2009.09.010.
Moore, V.M., Vendeville, B.C., Wiltschko, D.V., 2005a. Effects of buoyancy and mechanical layering on collisional deformation of continental lithosphere: results from physical modeling. Tectonophysics 403, 193–222, http://dx.doi.org/10.1016/j.tecto.2005.04.004.
Moore, V.M., Vendeville, B.C., Wiltschko, D.V., 2005b. Effects of buoyancy and mechanical layering on collisional deformation of continental lithosphere: results from physical modeling. Tectonophysics 403, 193–222, http://dx.doi.org/10.1016/j.tecto.2005.04.004.
Moresi, L., Gurnis, M., 1996. Constraints on the lateral strength of slabs from three-dimensional dynamic flow models. Earth Planet. Sci. Lett. 138, 15–28.
Mourgues, R., Lecomte, E., Vendeville, B., Raillard, S., 2009. An experimental investigation of gravity-driven shale tectonics in progradational delta. Tectonophysics 474, 643–656, http://dx.doi.org/10.1016/j.tecto.2009.05.003.
Muñoz, J.A., 1992. Evolution of a continental collision belt: ECORS-Pyrenees crustal balanced cross-section. In: McClay, K.R. (Ed.), Thrust Tectonics. Chapmann and Hall, London, pp. 235–246.
Mugnier, J.L., Baby, P., Colletta, B., Vinour, P., Bale, P., Leturmy, P., 1997. Thrust geometry controlled by erosion and sedimentation: a view from analogue models. Geology 25, 427–430.
Munteanu, I., Willingshofer, E., Sokoutis, D., Matenco, L., Dinu, C., Cloetingh, S., 2013. Transfer of deformation in back-arc basins with a laterally variable rheology: constraints from analogue modelling of the Balkanides–Western Black Sea inversion. Tectonophysics 602, 223–236.
Nalpas, T., Brun, J.P., 1993. Salt flow and diapirism related to extension at crustal scale. Tectonophysics 228, 349–362.
Naylor, M.A., Mandl, G., Sijpesteijn, C.H.K., 1986. Fault geometries in basement-induced wrench faulting under different initial stress states. J. Struct. Geol. 8, 737–752.
Neurath, C., Smith, R.B., 1982. The effect of material properties on growth rates of folding and boudinage: experiments with wax models. J. Struct. Geol. 4, 215–229.
Nilforoushan, F., Koyi, H.A., 2007. Displacement fields and finite strains in a sandbox model simulating a fold-thrust-belt. Geophys. J. Int. 169, 1341–1355, http://dx.doi.org/10.1111/j.1365-246X.2007.03341.x.
Noble, T.E., Dixon, J.M., 2011. Structural evolution of fold-thrust structures in analog models deformed in a large geotechnical centrifuge. J. Struct. Geol. 33, 62–77, http://dx.doi.org/10.1016/j.jsg.2010.12.007.

Norini, G., Acocella, V., 2011. Analogue modeling of flank instability at Mount Etna: understanding the driving factors. J. Geophys. Res. 116, B07206, http://dx.doi.org/10.1029/2011jb008216.
Oertel, G., 1962. A progress report on stress, strain and fracture in clay models of geologic deformation. Geotimes 6, 26–31.
Olson, P., Kincaid, C., 1991. Experiments on the interaction of thermal convection and compositional layering at the base of the mantle. J. Geophys. Res. 96, 4347–4354.
Panien, M., Schreurs, G., Pfiffner, A., 2006. Mechanical behaviour of granular materials used in analogue modelling: insights from grain characterisation, ring-shear tests and analogue experiments. J. Struct. Geol. 28, 1710–1724.
Parker, T.J., McDowell, A.N., 1955. Model studies of salt-dome tectonics. Bull. Am. Assoc. Petrol. Geol. 39, 2384–2470.
Passchier, C.W., Sokoutis, D., 1993. Experimental modelling of mantled porphyroclasts. J. Struct. Geol. 15, 895–909.
Pastor-Galán, D., Gutiérrez-Alonso, G., Zulauf, G., Zanellan, F., 2012. Analogue modeling of lithospheric-scale orocline buckling: constraints on the evolution of the Iberian-Armorican Arc. Geol. Soc. Am. Bull. 124, 1293–1309.
Paterson, M.S., 1978. Experimental Rock Deformation. Springer, New York.
Peltzer, G., Gillet, P., Tapponnier, P., 1984. Formation des failles dans un matériau modèle: la plasticine. Bulletin de la Société Géologique de France 26, 161–168.
Peltzer, G., 1988. Centrifuge experiments of continental scale tectonics in Asia. Bull. Geol. Inst. Univ. Uppsala 14, 115–128.
Perrin, C., Clemenzi, L., Malavieille, J., Molli, G., Taboada, A., Dominguez, S., 2013. Impact of erosion and décollements on large scale faulting and folding in orogenic wedges: analogue models and case studies. Journal of the Geological Society London 170, 893–904, http://dx.doi.org/10.1144/0016-76492013-012.
Platz, T., Münn, S., Walter, T.R., Procter, J.N., McGuire, P.C., Dumke, A., Neukum, G., 2011. Vertical and lateral collapse of tharsis tholus, mars. Earth Planet. Sci. Lett. 305, 445–455.
Précigout, J., Gueydan, F., 2009. Mantle weakening and strain localization: implications for the long-term strength of the continental lithosphere. Geology 37, 147–150.
Raffel, M., Willert, C.E., Wereley, S.T., Kompenhans, J., 2007. Particle Image Velocimetry: A Practical Guide. Springer.
Ramón, M.J., Pueyo, E.L., Rodríguez-Pintó, A., Ros, L.H., Pocoví, A., Luis Briz, J., Carlos Ciria, J., 2013. A computed tomography approach for understanding 3D deformation patterns in complex folds. Tectonophysics 593, 57–72, http://dx.doi.org/10.1016/j.tecto.2013.02.027.
Ramberg, H., 1967. Model experimentation of the effect of gravity on tectonic processes. Geophys. J. R. Astron. Soc. 14, 307–329.
Ramberg, H., 1955. Natural and experimental boudinage and pinch-and-swell structures. J. Geol. 63, 512–526.
Ramberg, H., 1970. Model studies in relation to intrusion of plutonic bodies, in: Newall, G., Rast, N. (Eds.), Mechanism of igneous intrusion, 2 ed, pp. 261–286.
Ramberg, H., 1981. Gravity. In: Deformation and the Earth's Crust, second ed. Academic Press, London.
Ranalli, G., 2001. Experimental tectonics: from Sir James Hall to the present. J. Geodyn. 32, 65–76.
Ratschbacher, L., Merle, O., Davy, P., Cobbold, P., 1991. Lateral extrusion in the Eastern Alps; Part 1, Boundary conditions and experiments scaled for gravity. Tectonics 10, 245–256.
Regard, V., Faccenna, C., Martinod, J., Bellier, O., Thomas, J.-C., 2003. From subduction to collision: control of deep processes on the evolution of convergent plate boundary. J. Geophys. Res. 108 (2208), 2210, http://dx.doi.org/10.1029/2002jb001943.
Regard, V., Faccenna, C., Martinod, J., Bellier, O., 2005. Slab pull and indentation tectonics: insights from 3D laboratory experiments. Phys. Earth Planet. Interiors 149, 99–113, http://dx.doi.org/10.1016/j.pepi.2004.08.011.
Ribe, N.M., Davaille, A., 2013. Dynamical similarity and density (non-) proportionality in experimental tectonics. Tectonophysics 608, 1371–1379.
Ribe, N.M., 2010. Bending mechanics and mode selection in free subduction: a thin-sheet analysis. Geophys. J. Int. 180, 559–576, http://dx.doi.org/10.1111/j.1365-246X.2009.04460.x.
Richard, P., 1991. Experiments on faulting in a two-layered cover sequence overlying a reactivated basement fault with oblique-slip. J. Struct. Geol. 13, 459–469.
Richefeu, V., El Youssoufi, M.S., Radjai, F., 2006. Shear strength properties of wet granular materials. Phys. Rev. 73, 051304.
Richter, F.M., Parsons, B., 1975. On the interaction of two scales of convection in the mantle. J. Geophys. Res. 80, 2529–2541.
Riller, U., Boutelier, D., Schrank, C., Cruden, A.R., 2010. Role of kilometer-scale weak circular heterogeneities on upper crustal deformation patterns: evidence from scaled analogue modeling and the Sudbury Basin Canada. Earth and Planet. Sci. Lett. 297, 587–597.
Rivalta, E., Taisne, B., Bunger, A.P., Katz, R.F., 2015. A review of mechanical models of dike propagation: schools of thought, results and future directions. Tectonophysics 638, 1–42, http://dx.doi.org/10.1016/j.tecto.2014.10.003.
Rosas, F., Marques, F.O., Luz, A., Coelho, S., 2002. Sheath folds formed by drag induced by rotation of rigid inclusions in viscous simple shear flow: nature and experiments. J. Struct. Geol. 24, 45–55.
Rosas, F.M., Duarte, J.C., Neves, M.C., Terrinha, P., Silva, S., Matias, L., Gràcia, E., Bartolome, R., 2012. Thrust-wrench interference between major active faults in the Gulf of Cadiz (Africa-Eurasia plate boundary, offshore SW Iberia): Tectonic implications from coupled analog and numerical modeling. Tectonophysics 548-549, 1–21, http://dx.doi.org/10.1016/j.tecto.2012.04.013.
Rosas, F.M., Duarte, J.C., Schellart, W.P., Tomás, R., Grigorova, V., Terrinha, P., 2015. Analogue modelling of different angle thrust-wrench fault interference in a brittle medium. J. Struct. Geol. 74, 81–104, http://dx.doi.org/10.1016/j.jsg.2015.03.005.
Rosenau, M., Lohrmann, J., Oncken, O., 2009. Shocks in a box: an analogue model of subduction earthquake cycles with application to seismotectonic forearc evolution. J. Geophys. Res. 114, B01409, http://dx.doi.org/10.1029/2008jb005665.
Rossetti, F., Ranalli, G., Faccenna, C., 1999. Rheological properties of paraffin as an analogue material for viscous crustal deformation. J. Struct. Geol. 21, 413–417.
Rossetti, F., Faccenna, C., Ranalli, G., Storti, F., 2000. Convergence rate-dependent growth of experimental viscous orogenic wedges. Earth Planet. Sci. Lett. 178, 367–372.
Rossi, D., Storti, F., 2003. New artificial granular materials for analogue laboratory experiments: aluminium and siliceous microspheres. J. Struct. Geol. 25, 1893–1899.
Schöpfer, M.P.J., Zulauf, G., 2002. Strain dependent rheology and the memory of plasticine. Tectonophysics 354, 85–99.
Schöpfer, M.P., Childs, C., Walsh, J.J., Manzocchi, T., Koyi, H.A., 2007. Geometrical analysis of the refraction and segmentation of normal faults in periodically layered sequences. J. Struct. Geol. 29, 318–335.
Schardt, H., 1884. Geological studies in the pays-D'Enhant vaudois. Bull. de le Soc. Vaudois des Sci. Nat., 143–146.
Schellart, W.P., Lister, G.S., 2005. The role of the East Asian active margin in widespread extensional and strike-slip deformation in East Asia. J. Geol. Soc. Lond. 162, 959–972, http://dx.doi.org/10.1144/0016-764904-112.
Schellart, W.P., Nieuwland, D.A., 2003. 3D evolution of a pop-up structure above a double basement strike-slip fault: some insights from analogue modelling. In: Nieuwland, D.A. (Ed.), New Insights into Structural Interpretation and Modelling. Bath, pp. 169–179.
Schellart, W.P., Lister, G.S., Jessell, M.W., 2002a. Analogue modelling of asymmetrical back-arc extension. J. Virtual Explorer 7, 25–42, http://dx.doi.org/10.3809/jvirtex.2002.00046.
Schellart, W.P., Lister, G.S., Jessell, M.W., 2002b. Analogue modeling of arc and backarc deformation in the New Hebrides arc and North Fiji Basin. Geology 30, 311–314, http://dx.doi.org/10.1130/0091-7613(2002)030<0311:AMOAAB>2.0.CO;2.
Schellart, W.P., Jessell, M.W., Lister, G.S., 2003. Asymmetric deformation in the backarc region of the Kuril arc, northwest Pacific: new insights from analogue modeling. Tectonics 22 (5), 1047, http://dx.doi.org/10.1029/2002tc001473.
Schellart, W.P., Freeman, J., Stegman, D.R., Moresi, L., May, D., 2007. Evolution and diversity of subduction zones controlled by slab width. Nature 446, 308–311, http://dx.doi.org/10.1038/nature05615.
Schellart, W.P., 2000. Shear test results for cohesion and friction coefficients for different granular materials: scaling implications for their usage in analogue modelling. Tectonophysics 324, 1–16, http://dx.doi.org/10.1016/S0040-1951(00)00111-6.
Schellart, W.P., 2002. Analogue modelling of large-scale tectonic processes: an introduction. J. Virtual Explor. 7, 1–6, http://dx.doi.org/10.3809/jvirtex.2002.00045.
Schellart, W.P., 2004a. Kinematics of subduction and subduction-induced flow in the upper mantle. J. Geophys. Res. 109, B07401, http://dx.doi.org/10.1029/2004jb002970.
Schellart, W.P., 2004b. Quantifying the net slab pull force as a driving mechanism for plate tectonics. Geophys. Res. Lett. 31, L07611, http://dx.doi.org/10.01029/02004GL019528.
Schellart, W.P., 2005. Influence of the subducting plate velocity on the geometry of the slab and migration of the subduction hinge. Earth Planet. Sci. Lett. 231, 197–219, http://dx.doi.org/10.1016/j.epsl.2004.12.019.
Schellart, W.P., 2008. Kinematics and flow patterns in deep mantle and upper mantle subduction models: influence of the mantle depth and slab to mantle viscosity ratio. Geochem. Geophys. Geosyst. 9, Q03014, http://dx.doi.org/10.1029/2007gc001656.
Schellart, W.P., 2010a. Evolution of subduction zone curvature and its dependence on the trench velocity and the slab to upper mantle viscosity ratio. J. Geophys. Res. 115, B11406, http://dx.doi.org/10.1029/2009jb006643.
Schellart, W.P., 2010b. Mount Etna–Iblean volcanism caused by rollback-induced upper mantle upwelling around the Ionian slab edge: an alternative to the plume model. Geology 38, 691–694, http://dx.doi.org/10.1130/G31037.1.
Schellart, W.P., 2011. Rheology and density of glucose syrup and honey: determining their suitability for usage in analogue and fluid dynamic models of geological processes. J. Struct. Geol. 33, 1079–1088, http://dx.doi.org/10.1016/j.jsg.2011.03.013.
Schrank, C.E., Cruden, A.R., 2010. Compaction control of topography and fault network structure along strike-slip faults in sedimentary basins. J. Struct. Geol. 32, 184–191.
Schrank, C.E., Boutelier, D.A., Cruden, A.R., 2008. The analogue shear zone: from rheology to associated geometry. J. Struct. Geol. 30, 177–193.
Schreurs, G., Hänni, R., Vock, P., 2001. Four-dimensional analysis of analogue models: experiments on transfer zones in fold and thrust belts. In: Koyi, H.A., Mancktelow, N.S. (Eds.), Tectonic Modelling: A Volume in Honor of Hans Ramberg. , pp. 179–190.
Schreurs, G., Buiter, S.J.H., Boutelier, D., Corti, G., Costa, E., Cruden, A.R., Daniel, J.-M., Hoth, S., Koyi, H., Kukowski, N., Lohrmann, J., Ravaglia, A., Schlische, R.W., Withjack, M.O., Yamada, Y., Cavozzi, C., DelVentisetti, C., Elder Brady, J.A., Hoffmann-Rother, A., Mengus, J.-M., Montanari, D., Nilforoushan, F., 2006.

Analogue benchmarks of shortening and extension experiments. Geol. Soc. Lond. Special Publ. 253, 1–27.
Schreurs, G., Buiter, S.J.H., Boutelier, J., Burberry, C., Callot, J.-P., Cavozzi, C., Cerca, M., Chen, J.-H., Cristallini, E., Cruden, A.R., Cruz, L., Daniel, J.-M., Da Poian, G., Garcia, V.H., Gomes, C.J.S., Grall, C., Guillot, Y., Guzmán, C., Nur Hidayah, T., Hilley, G., Klinkmüller, M., Koyi, H.A., Lu, C.-Y., Maillot, B., Meriaux, C., Nilfouroushan, F., Pan, C.-C., Pillot, D., Portillo, R., Rosenau, M., Schellart, W.P., Schlische, R.W., Take, A., Vendeville, B., Vergnaud, M., Vettori, M., Wang, S.-H., Withjack, M.O., Yagupsky, D., Yamada, Y., 2016. Benchmarking analogue models of brittle thrust wedges. J. Struct. Geol., http://dx.doi.org/10.1016/j.jsg.2016.03.005 (in Press).
Schreurs, G., 1994. Experiments on strike-slip faulting and block rotation. Geology 22, 567–570.
Schueller, S., Davy, P., 2008. Gravity influenced brittle-ductile deformation and growth faulting in the lithosphere during collision: results from laboratory experiments. J. Geophys. Res. 113, B12404, http://dx.doi.org/10.1029/2007jb005560.
Shemenda, A.I., Grocholsky, A.L., 1994. Physical modeling of slow seafloor spreading. J. Geophys. Res. 99, 9137–9153.
Shemenda, A.I., 1983. Similarity Criteria in Mechanical Modeling of Tectonic Processes Soviet. Geol. Geophys. 24, 8–16.
Shemenda, A.I., 1992. Horizontal lithosphere compression and subduction: constraints provided by physical modeling. J. Geophys. Res. 97, 11097–11116.
Shemenda, A.I., 1993. Subduction of the lithosphere and back arc dynamics: insights from physical modeling. J. Geophys. Res. 98, 16167–16185.
Sherlock, D.H., Evans, B.J., 2001. The development of seismic reflection sandbox modeling. AAPG Bull. 85, 1645–1659.
Sokoutis, D., Burg, J.P., Bonini, M., Corti, G., Cloetingh, S., 2005. Lithospheric-scale structures from the perspective of analogue continental collision. Tectonophysics 406, 1–15.
Storti, F., Salvini, F., McClay, K., 1997. Fault-related folding in sandbox analogue models of thrust wedges. J. Struct. Geol. 19, 583–602.
Storti, F., Salvini, F., McClay, K., 2000. Synchronous and velocity-partitioned thrusting and thrust polarity reversal in experimentally produced, doubly-vergent thrust wedges: implications for natural orogens. Tectonics 19, 378–396.
Storti, F., Marín, R.S., Rossetti, F., Casas Sainz, A.M., 2007. Evolution of experimental thrust wedges accreted from along-strike tapered, silicone-floored multilayers. J. Geol. Soc. Lond. 164, 73–85.
Strak, V., Schellart, W.P., 2014. Evolution of 3-D subduction-induced mantle flow around lateral slab edges in analogue models of free subduction analysed by stereoscopic particle image velocimetry technique. Earth Planet. Sci. Lett. 403, 368–379, http://dx.doi.org/10.1016/j.epsl.2014.07.007.
Strak, V., Schellart, W.P., 2016. Control of slab width on subduction-induced upper mantle flow and associated upwellings: Insights from analog models. J. Geophys. Res., 121, http://dx.doi.org/10.1002/2015JB012545.
Strak, V., Dominguez, S., Petit, C., Meyer, B., Loget, N., 2011. Interaction between normal fault slip and erosion on relief evolution: insights from experimental modelling. Tectonophysics 513, 1–19, http://dx.doi.org/10.1016/j.tecto.2011.10.005.
Tapponnier, R., Peltzer, G., Le Dain, A.Y., Armijo, R., Cobbold, P., 1982. Propagating extrusion tectonics in Asia; new insights from simple experiments with plasticine. Geology 10, 611–616.
Teixell, A., Koyi, H.A., 2003. Experimental and field study of the effects of lithological contrasts on thrust-related deformation. Tectonics 22 (1054), http://dx.doi.org/10.1029/2002tc001407.
Tibaldi, A., Pasquarè, F.A., Papanikolaou, D., Nomikou, P., 2008. Tectonics of Nisyros Island, Greece, by field and offshore data, and analogue modelling. J. Struct. Geol. 30, 1489–1506, http://dx.doi.org/10.1016/j.jsg.2008.08.003.
Trubitsyn, V.P., 2012. Rheology of the mantle and tectonics of the oceanic lithospheric plates. Izv. Phys. Solid Earth 48, 467–485.
Vendeville, B.C., Jackson, M.P.A., 1992. The rise of diapirs during thin-skinned extension. Mar. Petrol. Geol. 9, 331–354.
Vendeville, B., Cobbold, P.R., Davy, P., Brun, J.P., Choukroune, P., 1987. Physical models of extensional tectonics at various scales. Geol. Soc. Lond. Special Publ. 28, 95–107.
Viaplana-Muzas, M., Babault, J., Dominguez, S., Van Den Driessche, J., Legrand, X., 2015. Drainage network evolution and patterns of sedimentation in an experimental wedge. Tectonophysics 664, 109–124.
Vilotte, J.P., Daignieres, M., Madariaga, R., 1982. Numerical modeling of intraplate deformation: simple mechanical models of continental collision. J. Geophys. Res. 87, 10709–10728.
Wang, J.N., Hobbs, B.E., Or, d., Shimanioto, A., Toriumi, T., 1994. Newtonian dislocation creep in quartzites: implications for the rheology of the lower crust. Science 165, 1204–1206.
Warsitzka, M., Kley, J., Kukowski, N., 2013. Salt diapirism driven by differential loading — Some insights from analogue modelling. Tectonophysics 591, 83–97, http://dx.doi.org/10.1016/j.tecto.2011.11.018.
Weeraratne, D., Manga, M., 1998. Transitions in the style of mantle convection at high Rayleigh number. Earth Planet. Sci. Lett. 160, 563–568.
Weertman, J., 1978. Creep laws for the mantle of the earth. Philos. Trans. R. Soc. Lond. A 288, 9–26.
Weijermars, R., Schmeling, H., 1986. Scaling of Newtonian and non-Newtonian fluid dynamics without inertia for quantitative modelling of rock flow due to gravity (including the concept of rheological similarity). Phys. Earth Planet. Interiors 43, 316–330.
Weijermars, R., 1986. Flow behaviour and physical chemistry of bouncing putties and related polymers in view of tectonic laboratory applications. Tectonophysics 124, 325–358.
Weinstein, S.A., Christensen, U., 1991. Convection planforms in a fluid with a temperature-dependent viscosity beneath a stress-free upper boundary. Geophys. Res. Lett. 18, 2035–2038.
Weinstein, S.A., Olson, P., 1990. Planforms in thermal convection with internal heat sources at large Rayleigh and Prandtl numbers. Geophys. Res. Lett. 17, 239–242.
White, D.B., 1988. The planforms and onset of convection with a temperature-dependent viscosity. J. Fluid Mech. 191, 247–286.
Whitehead, J.A., Luther, D.S., 1975. Dynamics of laboratory diapir and plume models. J. Geophys. Res. 80, 705–717.
Willingshofer, E., Sokoutis, D., 2009. Decoupling along plate boundaries: key variable controlling the mode of deformation and the geometry of collisional mountain belts. Geology 37, 39–42, http://dx.doi.org/10.1130/G25321A.1.
Willingshofer, E., Sokoutis, D., Luth, S.W., Beekman, F., Cloetingh, S., 2013. Subduction and deformation of the continental lithosphere in response to plate and crust-mantle coupling. Geology 41, 1239–1242.
Willis, B., 1893. Part 2; The Mechanics of Appalachian Structure. United States Geological Survey Annual Report 13211–281 (Part 2).
Yamada, Y., Baba, K., Matsuoka, T., 2006. Analogue and numerical modelling of accretionary prisms with a decollement in sediments. In: Buiter, S.J.H., Schreurs, G. (Eds.), Analogue and Numerical Modelling of Crustal-Scale Processes. Geological Society, London.
Zhang, K.J., Cai, J.X., Zhu, J.X., 2006. North China and South China collision: insights from analogue modeling. J. Geodyn. 42, 38–51.
Zulauf, J., Zulauf, G., 2004. Rheology of plasticine used as rock analogue: the impact of temperature, composition and strain. J. Struct. Geol. 26, 725–737.
Zulauf, G., Zulauf, J., Hastreiter, P., Tomandl, B., 2003. A deformation apparatus for three-dimensional coaxial deformation and its application to rheologically stratified analogue material. J. Struct. Geol. 25, 469–480.
Zulauf, J., Zulauf, G., Kraus, R., Gutiérrez-Alonso, G., Zanella, F., 2011. The origin of tablet boudinage: results from experiments using power–law rock analogs. Tectonophysics 510, 327–336, http://dx.doi.org/10.1016/j.tecto.2011.07.013.
ten Grotenhuis, S.M., Piazolo, S., Pakula, T., Passchier, C.W., Bons, P.D., 2002. Are polymers suitable rock analogs ? Tectonophysics 350, 35–47.
van Mechelen, J.L.M., 2004. Strength of moist sand controlled by surface tension for tectonic analogue modelling. Tectonophysics 384, 275–284.